

1           **A RAF-like kinase mediates a deeply conserved, ultra-rapid auxin response**

2

3           Andre Kuhn<sup>1,\*</sup>, Mark Roosjen<sup>1,\*</sup>, Sumanth Mutte<sup>1</sup>, Shiv Mani Dubey<sup>2</sup>, Polet Carrillo  
4           Carrasco<sup>1</sup>, Aline Monzer<sup>3</sup>, Takayuki Kohchi<sup>4</sup>, Ryuichi Nishihama<sup>5</sup>, Matyáš Fendrych<sup>2</sup>, Jiří  
5           Friml<sup>3</sup>, Joris Sprakel<sup>1,6</sup> and Dolf Weijers<sup>1,#</sup>

6

7           1, Laboratory of Biochemistry, Wageningen University, Stippeneng 4, Wageningen, the  
8           Netherlands

9           2, Department of Experimental Plant Biology, Charles University, Prague

10           3, Institute of Science and Technology Austria, Klosterneuburg, Austria

11           4, Graduate School of Biostudies, Kyoto University, Kyoto, Japan

12           5, Department of Applied Biological Science, Faculty of Science and Technology Tokyo  
13           University of Science, Noda, Chiba, Japan

14           6, Laboratory of Physical Chemistry and Soft Matter, Wageningen University, Wageningen,  
15           the Netherlands

16

17           \*, these authors contributed equally

18           #, corresponding author: [dolf.weijers@wur.nl](mailto:dolf.weijers@wur.nl)

19

20           Lead Contact: Further information and requests for resources and reagents should be directed  
21           to and will be fulfilled by the lead contact, Dolf Weijers ([dolf.weijers@wur.nl](mailto:dolf.weijers@wur.nl)).

22

23

24

25

26

27

28

29 **SUMMARY**

30

31 The plant signaling molecule auxin triggers both fast and slow cellular responses across the  
32 plant kingdom, including both land plants and algae. A nuclear response pathway mediates  
33 auxin-dependent gene expression, and controls a range of growth and developmental  
34 processes in land plants. It is unknown what mechanisms underlie both the physiological  
35 responses occurring within seconds, and the responses in algae, that lack the nuclear auxin  
36 response pathway. We discovered an ultra-fast proteome-wide phosphorylation response to  
37 auxin across 5 land plant and algal species, converging on a core group of shared target  
38 proteins. We find conserved rapid physiological responses to auxin in the same species and  
39 identified a RAF-like protein kinase as a central mediator of auxin-triggered phosphorylation  
40 across species. Genetic analysis allowed to connect this kinase to both auxin-triggered protein  
41 phosphorylation and a rapid cellular response, thus identifying an ancient mechanism for fast  
42 auxin responses in the green lineage.

43

44

45

46 **KEYWORDS**

47

48 Auxin, protein phosphorylation, RAF kinase, plant evolution

49

50

51 **INTRODUCTION**

52

53 The plant signaling molecule is key to numerous growth and developmental processes in  
54 plants<sup>1</sup>. Iconic auxin-dependent processes are the tropic growth responses to light and  
55 gravity<sup>2-5</sup>, differentiation of vascular strands and the control of fruit development<sup>6-9</sup>. The  
56 dominant naturally occurring auxin is indole 3-acetic acid (IAA), a chemically simple  
57 Tryptophan derivative that land plants can synthesize in a two-step pathway, but that is widely  
58 found across both prokaryotic and eukaryotic species<sup>10</sup>. While initial discoveries with auxin  
59 were made in flowering plants, both the occurrence of IAA and physiological and  
60 developmental responses to the molecule have been reported well beyond this group. All land  
61 plants studied<sup>11</sup>, and a range of algae<sup>12-14</sup> show responses to externally applied auxin, which  
62 suggests a very deep origin of the capacity to respond to auxin. The cellular responses to  
63 auxin come in essentially two flavors: fast and slow. The fast responses include changes in  
64 membrane polarization<sup>15-17</sup>, cytoplasmic streaming<sup>18,19</sup>, Calcium and proton fluxes<sup>20-24</sup> and  
65 remodeling of the cytoskeleton<sup>12,25</sup> and trafficking<sup>26</sup>. Slower responses include cellular  
66 growth, division and differentiation<sup>27-30</sup>.

67 Following an era of biochemical investigation that led to the identification of a set of  
68 auxin-binding proteins<sup>31</sup>, genetic approaches have been incredibly successful in defining a  
69 comprehensive response system. Using the ability of auxin to inhibit root growth in the  
70 flowering plant *Arabidopsis thaliana* as a model, a set of components was identified that  
71 mediates auxin's activity in regulating gene expression – the nuclear auxin pathway (NAP)<sup>32-36</sup>. This system revolves around the auxin-triggered proteolysis of a family of transcriptional  
72 repressor proteins, thus liberating DNA-bound transcription factors and allowing gene  
73 regulation<sup>37</sup>. Through this pathway, auxin controls the expression of hundreds-thousands of  
74 genes, and mutations in its components interfere with most, if not all developmental auxin  
75 functions, culminating in embryo lethality in the most affected mutants<sup>38-40</sup>.

77 As increasing numbers of plant genomes have become available, it became possible to  
78 reconstruct the occurrence and evolutionary history of the auxin response system. From such  
79 analysis, it appeared that the same auxin response system acts to control gene expression and  
80 development across land plants<sup>11,41</sup>. However, it is also clear that the closest sister group to  
81 land plants – the streptophyte algae – do not carry the NAP, in cases even lacking all its  
82 components<sup>11</sup>. Thus, a major unanswered question is how algae can respond to auxin in the  
83 absence of the known auxin response system. In addition, the fastest gene expression

84 responses to auxin have been recorded in 5-10 minutes<sup>42,43</sup>, but several of the fast  
85 responses<sup>18,19,23,44,45</sup> occur within seconds, or at least well within the time needed for gene  
86 expression and protein synthesis. Thus, it is likely that the currently known auxin response  
87 system represents the “slow” branch, and that a separate, currently unknown system must  
88 exist to mediate fast responses. The existence of fast auxin responses in land plants and their  
89 algal sisters would predict such a system to be shared between these clades.

90 Building on the rich literature in animal signaling, we explored the hypothesis that  
91 regulated protein phosphorylation may represent a mechanism mediating fast auxin responses.  
92 In the accompanying article (Roosjen, Kuhn et al., accompanying manuscript) we  
93 demonstrate that auxin can trigger changes in protein phosphorylation well within 30 seconds,  
94 and that more than 2000 proteins are targeted by auxin-triggered phosphorylation within 10  
95 minutes in *Arabidopsis* roots. Auxin-triggered phosphorylation targets numerous pathways,  
96 including those leading to changes in membrane polarity. Here, we asked if this novel auxin  
97 response may represent the elusive, deeply conserved mechanism underlying rapid cellular  
98 responses. We indeed find that auxin triggers rapid changes in protein phosphorylation in 5  
99 different land plant and algal species, including a core set of conserved targets. We show that  
100 auxin has deeply conserved activity in accelerating cytoplasmic streaming and membrane  
101 polarity. Lastly, we identify a key RAF-like kinase that mediates auxin-triggered protein  
102 phosphorylation and control of fast cellular responses across species. This work thus identifies  
103 an ancient system for rapid responses to the auxin signaling molecule.

104

105 **RESULTS**

106

107 **Identification of a deeply conserved, rapid, phosphorylation-based auxin response**

108

109 To examine whether the rapid phosphorylation-based auxin response that we have identified  
110 in *Arabidopsis thaliana* roots (Henceforth: Arabidopsis; Roosjen, Kuhn et al, accompanying  
111 manuscript) is conserved beyond this species, we selected a set of phylogenetically distant  
112 species ranging from green algae to bryophytes for phosphoproteomic analysis. These  
113 included the streptophyte algae *Klebsormidium nitens* (Klebsormidium) and *Penium*  
114 *margaritaceum* (Penium) and the bryophytes *Marchantia polymorpha* (Marchantia) and  
115 *Physcomitrium patens* (Physcomitrium) in addition to the angiosperm Arabidopsis. This  
116 selection encompasses both early-diverging streptophyte algae (Klebsormidium) and a close  
117 sister to land plants (Penium; Zygnematophyceae), and covers two clades within the  
118 bryophytes: liverworts (Marchantia) and mosses (Physcomitrium). Notably, while sporophytic  
119 (root) tissue was sampled for Arabidopsis, gametophyte tissue was sampled for all other  
120 species. Thus, the suite of species not only spans phylogeny, but also haploid and diploid  
121 generations. All species were treated with the same concentration (100 nM) of the naturally  
122 occurring auxin Indole 3-Acetic Acid (IAA, auxin), followed by phosphopeptide enrichment  
123 after two minutes using the same experimental, mass spectrometry and analysis workflow that  
124 we describe in Roosjen, Kuhn et al. (accompanying manuscript). Strikingly, we find that two  
125 minutes of auxin treatment leads to large shifts in the phospho-proteome in all species tested  
126 (Figure 1A). The number of differential phosphosites was comparable across species  
127 (FDR $\geq$ 1.301: n=1048 in Arabidopsis; n=670 in Physcomitrium; n=741 in Marchantia; n=719  
128 in Penium; n=1231 in Klebsormidium). In all species except Klebsormidium,  
129 hyperphosphorylation upon auxin treatment represented the majority of differential  
130 phosphosites (64% in Arabidopsis, 76% in Physcomitrium, 73% in Marchantia and 60% in  
131 Penium), while hyper- and hypophosphorylation were more equal in Klebsormidium (47%  
132 hyperphosphorylation) (Figure 1A). Thus, rapid, global changes in phospho-proteomes are  
133 triggered by auxin at comparable scale in all species tested.

134

135 We next asked if the cellular functions and proteins that are targeted by auxin-  
136 triggered phosphorylation changes are conserved among the species tested. Estimated  
137 divergence times of the species used here from common ancestors is around 850 Mya for  
138 algae and land plants, and 500 Mya among the land plants<sup>46</sup>. Given these enormous  
evolutionary distances, there is substantial sequence divergence within protein families, and

139 large differences in gene family numbers<sup>47</sup>. This makes establishing direct orthology  
140 relationships very challenging. Therefore, before comparison of differential phosphoproteins  
141 at protein/family level, we first constructed a set of orthogroups that represent the set of genes  
142 that originated from a single gene in the last common ancestor of all the species under  
143 consideration. We then consider members of the same orthogroup to represent a conserved  
144 ancestral function. Among the species tested, *Penium* has a remarkably large number of  
145 orthogroups with multiple members within *Penium* (Figure 1B), which is a reflection of the  
146 high degree of fragmentation of the genome assembly<sup>48</sup>.

147 Comparing the phosphosites in all species, we found an overlap of 11 orthogroups  
148 across all organisms (Figure 1C). Given the previous consideration, we also consider  
149 orthogroups not represented in *Penium* to be relevant. When excluding *Penium* from the  
150 analysis we found 29 orthogroups to be shared (Figure 1C). Gene Ontology (GO) analysis on  
151 the conserved orthogroups showed that a broad range of cellular functions is subject to auxin  
152 regulation (Figure 1D). These include processes at the plasma membrane or endomembranes,  
153 such as transmembrane transport and clathrin coat disassembly, but also nuclear organization  
154 and posttranslational regulation of gene expression. Furthermore, GO analysis identified  
155 responses to external stimuli and hormones, including response to blue light, abscisic acid  
156 transport and polar auxin transport. As expected from a phospho-proteomic analysis, protein  
157 phosphorylation was another highly enriched GO-term. In line with that, we find RAF-like  
158 kinases and the blue-light receptor PHOT1 as a conserved target of auxin-triggered  
159 phosphorylation (Figure 1E).

160 Limiting GO analysis to only the 29 conserved orthogroups is very stringent, as it is  
161 strongly constrained by sequence similarity, which may be limited across such long  
162 evolutionary timescales. We therefore also performed GO analysis on the full set of  
163 differentially phosphorylated phosphosites (FDR≤0,05) in each species separately, and  
164 compared the enriched GO-terms. This comparison found 7 GO-terms enriched in all species  
165 tested (Figure 1F), suggesting that these represent core target processes of rapid auxin  
166 response. Beyond the previously identified GO terms (Figure 1D), “transmembrane transport”  
167 and “proton transmembrane transport” were highly enriched (Figure 1G). Further analysis  
168 showed that in all species tested, H<sup>+</sup>-ATPase proton pumps were differentially phospho-  
169 regulated upon auxin treatment (Figure 1H). Clearly, there were also many GO-terms that  
170 were uniquely enriched in one or a few species (Figure 1F), suggesting that rapid auxin-  
171 triggered phosphorylation not only has a conserved component, but also a species/lineage-

172 specific component. In conclusion, auxin triggers a conserved set of rapid phosphorylation  
173 changes across land plants and algae, converging on shared cellular processes.

174

## 175 **Auxin triggers fast cellular and physiological responses across the plant lineage**

176

177 The identification of a deeply conserved auxin response that targets a common set of proteins  
178 and functions, suggests that there are cellular processes that auxin can regulate across the  
179 green kingdom. Among the fast auxin responses that have previously been recorded (see  
180 introduction), two stand out as being potential candidates for being shared outside of land  
181 plants. We explored whether auxin can trigger changes in membrane polarity and cytoplasmic  
182 streaming across species.

183 Membrane potential reflects the difference between cytoplasmic and apoplastic  
184 electrical potentials (Figure 2A). Auxin has a profound effect on membrane potential by  
185 triggering instantaneous depolarization of plasma membranes. This depolarization is then  
186 followed by a hyperpolarization of the membrane<sup>17,24</sup>. Both membrane depolarization and  
187 hyperpolarization depend on auxin's ability to regulate ion fluxes across the plasma  
188 membrane, prominently involving H<sup>+</sup>-ATPase proton pumps<sup>17,23,49,50</sup>. To test whether this  
189 response is conserved in the plant lineage, we monitored membrane potential after 5 min of  
190 treatment with 100 nM auxin in *Arabidopsis* roots, *Marchantia gemmae* and *Klebsormidium*  
191 filaments using the membrane potential fluorescent probe DISBAC<sub>2</sub>(3)<sup>17,51</sup>. Increase in  
192 DISBAC<sub>2</sub>(3) fluorescence reports membrane depolarization<sup>17,51</sup>. We observed a significant  
193 increase of fluorescence ratio upon auxin-treatment in all three species (Figure 2A).  
194 Moreover, the increase was quantitatively very similar between species. This indicates that  
195 rapid auxin-triggered plasma membrane depolarization is a deeply conserved rapid auxin  
196 response.

197 Cytoplasmic streaming describes the movement of organelles along the actin  
198 cytoskeleton and is thought to have essential function in transport of nutrient and proteins  
199 within the cell<sup>52</sup>. In plants, cytoplasmic streaming is thought to be primarily driven by plant-  
200 specific Myosin XI cytoskeletal motor proteins<sup>52</sup>. We found that in *Arabidopsis*, Myosin XI-K  
201 and the MadB Myosin-binding proteins are targets of rapid auxin-dependent  
202 phosphorylation<sup>53</sup>, and that auxin promotes cytoplasmic streaming in root epidermal cells<sup>18</sup>.  
203 We examined the physiological effect of 100 nM auxin on cytoplasmic streaming by  
204 monitoring the movement of fluorescently labeled mitochondria in epidermis cells within the

205 root elongation zone in *Arabidopsis* and in *Marchantia* rhizoid cells (Figure 2B). After  
206 particle tracking, we determined the active diffusion rate (K) and diffusive exponent ( $\alpha$ ) by  
207 fitting mean-square displacements, ensemble-averaged per cell, to the anomalous diffusion  
208 model, in both auxin treated and untreated samples. We detected consistent streaming within  
209 both species, but found absolute rates to differ among species (Figure 2B). Pretreatment of  
210 *Arabidopsis* roots with the actin depolymerizing drug Latrunculin B reduced cytoplasmic  
211 streaming in both species (Supplementary Figure 1B), thus implicating the actin cytoskeleton.  
212 Importantly, auxin treatment increased the diffusion rate in all species tested (Figure 2B).  
213 Hence, like membrane depolarization, acceleration of cytoplasmic streaming is a deeply  
214 conserved cellular response to auxin.

215

## 216 **Identification of RAF-like kinases as conserved components in auxin response**

217

218 The finding that there are conserved phosphorylation responses to auxin in algae and land  
219 plants, along with conserved cellular responses, suggests the existence of a shared mechanism  
220 for auxin perception and signal transduction. Given the prominent phosphorylation changes  
221 across species and the temporal dynamics of the response in *Arabidopsis* (Roosjen, Kuhn et  
222 al, accompanying manuscript), we anticipate a key role for auxin-activated protein kinases. To  
223 identify such kinases, we first analyzed phosphorylation motifs enriched among the conserved  
224 phospho-targets. We found that hyperphosphorylation was associated with the presence of a  
225 proline-directed SP motif (Figure 3A). These are typically targeted by MAP kinases<sup>54,55</sup>.  
226 Indeed, when inferring kinase-target networks in *Arabidopsis* from temporal phosphorylation  
227 profiles and activation loop phosphorylation predictions, we identified an auxin-activated  
228 RAF-like Kinase as a potential hub, central to the phosphorylation network (Roosjen, Kuhn et  
229 al., accompanying manuscript). Strikingly, orthologues of this same Rapidly Accelerated  
230 Fibrosarcoma (RAF)-like kinase were hyperphosphorylated upon auxin treatment in all other  
231 species tested (Figure 1E and 3B), except in *Penium*, where genome assembly fragmentation  
232 likely precluded its identification. In addition to the RAF-like kinase, we also identified  
233 PHOT1 as a conserved target of auxin-triggered hyperphosphorylation (Figure 1E). However,  
234 given the multiple lines of evidence suggesting a role for the RAF-like Kinases in auxin-  
235 triggered phosphorylation, we here focus on this protein.

236 RAF-like kinases are serine/threonine kinases that belong to the mitogen activated  
237 protein kinase kinase kinases (MAPKKKs) family. They are classified into four B clades and  
238 seven C clades according to their homology with the widespread eukaryotic RAF protein

239 kinases<sup>56</sup>. *Arabidopsis* B2, B3 and B4 clade RAF-like kinases have been implicated in various  
240 physiological responses, including responses to hypoxia, osmotic stress and drought<sup>57,58</sup>. The  
241 *Marchantia* B4 RAF-like kinase (PRAF) was implicated in the regulation of carbon fixation<sup>59</sup>.  
242 While we found RAF-like kinases of the B2, B3 and B4 clade to be hyperphosphorylated after  
243 auxin treatment in *Arabidopsis*, it seems that only hyperphosphorylation of RAF-like kinases  
244 of the B3 and B4 clade upon auxin treatment is conserved (Figure 1E). The B4 clade is  
245 represented by 7 paralogs in *Arabidopsis*, 2 in *Physcomitrium* and single copies in  
246 *Klebsormidium* and *Marchantia*<sup>60</sup> (Figure 3C). Most of these are hyperphosphorylated in  
247 response to auxin treatment (Figure 3B), firmly connecting this family to auxin response. We  
248 refer to these proteins as MAP AUXIN RESPONSIVE KINASE/RAFs (MARK/RAFs).

249 Given that no role for these proteins in auxin response has been reported, we initially  
250 explored requirements for MARK/RAF kinases in auxin-associated growth and development,  
251 as well as in response to externally applied auxin. To this end, we analyzed previously  
252 established mutants: two septuple mutants of the entire *Arabidopsis* B4 clade either conferring  
253 a null (*mark/raf*<sup>null</sup>; also referred to as *OK*<sup>130</sup>-*null*<sup>58</sup>) or a weak allele combination  
254 (*mark/raf*<sup>weak</sup>; also referred to as *OK*<sup>130</sup>-*weak*<sup>58</sup>), and a null mutant in the single *Marchantia*  
255 ortholog (*Mpmark/praf*<sup>KO</sup>, also referred to as *Mppraf*<sup>KO</sup><sup>59</sup>). We found that in both species,  
256 loss of MARK activity caused growth and developmental phenotypes (Figure 3D). While in  
257 *Arabidopsis* we found a range of defects in root growth, plant height and rosette area and  
258 germination (Figure 3D; Supplementary Figure 2), in *Marchantia*, these manifested as smaller  
259 thallus size and reduced gemmae cup number confirming previously published results<sup>59</sup>  
260 (Figure 3D; Supplementary Figure 2). Essentially all these processes are known to involve  
261 auxin action<sup>30,61,62</sup>. We therefore tested sensitivity of the *Arabidopsis* and *Marchantia*  
262 *mark/praf* mutants to auxin. In *Arabidopsis*, *mark* mutant roots were slightly less sensitive to  
263 growth inhibition by auxin (Figure 3E). Likewise, *Marchantia* *mark/praf* mutant thallus,  
264 although already under control conditions reduced in size, was also less sensitive to auxin-  
265 induced growth inhibition (Figure 3F). Thus, in both species, MARK/RAF kinases act in  
266 growth and development, and play a role in auxin response.

267

## 268 **MARK kinases mediate fast auxin phospho-response**

269

270 Auxin-associated growth and development, as well as *Arabidopsis* root and *Marchantia*  
271 thallus growth responses to externally applied auxin is typically associated with changes in  
272 auxin-dependent gene expression through the NAP<sup>37,41</sup>. given the auxin-related phenotypes in

273 *mark* mutants, we asked if these are affected in transcriptional responses. We therefore  
274 performed RNA-Seq in *Arabidopsis* (roots) and *Marchantia* (thallus) wildtype and *mark/raf*  
275 mutants that were either treated with 1 $\mu$ M IAA or control medium for one hour. This  
276 concentration of IAA should allow to detect even subtle changes in transcription in mutants.  
277 In both species, transcriptomes under untreated conditions look very distinct between mutant  
278 and wildtype (Figure 4A,B), suggesting massive effects of loss of MARK/RAF function on  
279 the “baseline” transcriptome in the absence of externally applied auxin. However, comparing  
280 auxin-treated and untreated samples in both species showed substantial auxin-induced  
281 changes in transcriptomes in both wildtypes and in *mark/raf* mutants (Figure 4A,B).  
282 Qualitatively, mutants in both species still showed a typical gene expression response to  
283 auxin. Indeed, detailed analysis of individual auxin-regulated genes (Figure 4A,B) showed  
284 that mutants did not have an obvious defect in auxin-induced transcription. This suggests that  
285 MARK/RAF proteins do not have a major role in transcriptional auxin responses.

286 Given the rapid activation of MARK/RAF kinases by auxin (Figure 3B), it is  
287 conceivable that these kinases act in auxin response through their role in mediating rapid  
288 phosphorylation responses. We tested this hypothesis by subjecting *mark/raf* mutants in both  
289 *Arabidopsis* and *Marchantia* to phosphoproteomic profiling after two minutes of treatment  
290 with 100 nM IAA or control media. In both species, we found that the number of significant  
291 differential hyperphosphorylated phosphosites after auxin treatment was reduced (666 in  
292 *Arabidopsis* WT; 445 in *Atmark/raf* mutant; 538 in *Marchantia* WT; 285 in *Mpmark/praf*;  
293 Figure 4C). When comparing the number of phosphosites in wild-types and mutants, we  
294 found that 73% of the differential phosphosites in wild-type was lost in the *Arabidopsis*  
295 *mark/raf* mutant, while 51% was lost in the *Marchantia* *mark/praf* mutant (Figure 4C). We  
296 compared phosphoproteomes in non-treated mutants with wild-type controls in both species to  
297 identify functions that are deregulated in *mark* mutants. In *Arabidopsis* *mark/raf*, 392  
298 orthogroups were different between mutant and wildtype, while in *Marchantia* *mark/praf*, 785  
299 orthogroups were differentially phosphorylated (Figure 4D). Many orthogroups that were not  
300 significantly affected by auxin in wild-type became differentially phosphorylated upon auxin  
301 treatment in the mutants (Figure 4E). This suggests that the mutants in both species not only  
302 lack a substantial part of auxin-triggered phosphorylation, but also have a response system  
303 that is differently wired in non-treated conditions. This is consistent with the large  
304 transcriptional changes, and with the strong phenotypes in the mutants. When comparing  
305 targets of MARK-dependent, auxin-triggered phosphorylation changes in the two species, we  
306 found a small overlap (24 orthogroups; Figure 4E). Given the evolutionary distance between

307 Marchantia and Arabidopsis, this is remarkable since it suggests that there is indeed a set of  
308 evolutionary conserved fast auxin response under control of a conserved mechanism. These  
309 shared, MARK/auxin-dependent targets included proteins associated with a diverse set of  
310 cellular processes (Figure 4F; Supplementary Figure 3A). This includes ion transport,  
311 membrane dynamics, and auxin export (e.g. PIN's, ABCB's, D6PK), but also featured nuclear  
312 processes such as splicing and cytoplasmic processes such as cell plate formation and  
313 cytoskeleton organization (e.g. SPIKE1, TOR1, NEK5). Lastly, this analysis also identified  
314 previously reported phospho-targets of B4-type RAF kinases (e.g. VCS, VCR, SE).

315 To explore to what extent the auxin-triggered phosphorylation network is affected in  
316 *mark* mutants, we compared the phosphorylation state of all kinases that were significantly  
317 hypo- or hyperphosphorylated upon auxin treatment in wild-type of both species with their  
318 phosphorylation state in *mark* mutants. Notably, in *mark* mutants, most of the auxin-triggered  
319 kinase phosphorylation was lost (Figure 4G,H). This suggests that MARK/RAFs directly or  
320 indirectly regulates the auxin-triggered phosphorylation of these kinases.

321

## 322 **Specificity and mechanism of MARK activation**

323

324 Proteins in the Arabidopsis MARK/RAF family have been identified as being  
325 hyperphosphorylated upon osmotic treatment<sup>58</sup> and to mediate response to hypoxia<sup>57</sup>, while  
326 Marchantia MARK/PRAF has a role in the response to altered photosynthesis<sup>59</sup>. This suggests  
327 that the same kinase is part of multiple response pathways and urges the questions of how  
328 specific the auxin-triggered phosphorylation changes are, and how MARK/RAF is activated  
329 in the context of auxin response. We initially compared the 2-minute auxin-triggered  
330 phosphorylation changes with the set of 973 phosphosites that are osmotic stress-responsive  
331 in Arabidopsis<sup>58</sup>. The overlap was very limited (37 phosphosites; Supplementary Figure 3B),  
332 and 13 of these overlapping phosphosites depend on MARK/RAF (Supplementary Figure  
333 3B). We therefore conclude that the phosphoresponse that we identified here is specific and  
334 independent from osmotic stress responses.

335 We next explored mechanisms of MARK/RAF activation. In time-course  
336 phosphoproteome data (derived from Roosjen, Kuhn et al., accompanying manuscript), we  
337 found that multiple sites on all AtMARK/RAF proteins are modulated upon auxin treatment  
338 (Figure 5A), suggesting profound and rapid regulation. As part of our characterization of the  
339 auxin-triggered fast phosphoproteome in Arabidopsis, we found that the ABP1 auxin binding  
340 protein and the TMK1 receptor-like kinase as well as the intracellular AFB1 receptor

341 contribute to effects of auxin on the phosphoproteome (Friml et al., 2022; Roosjen, Kuhn et  
342 al., accompanying manuscript). We found that phosphoproteome changes in *abp1* and *tmk1*  
343 mutants are highly correlated (Roosjen, Kuhn et al., accompanying manuscript), while effects  
344 on the same phosphosites in *afb1* mutants often are anticorrelated (Roosjen, Kuhn et al.,  
345 accompanying manuscript). We compared the *Arabidopsis mark* mutant phosphoproteomes  
346 with those of wild type, *afb1*, *abp1* and *tmk1* mutants and found that phosphosites in *mark/raf*  
347 phosphoproteomes overlap less with those of *afb1-3* and the auxin-treated wildtype  
348 phosphoproteome than with those of *tmk1* and *abp1* (Figure 5B,D). This is true for both *mark*  
349 phosphoproteomes in control and auxin-treated conditions. suggesting that the *mark*  
350 phosphoproteome under mock conditions is already strongly distorted. Given that  
351 MARK/RAFs do not have a clear ligand-binding domain, we were interested to see if  
352 MARK/RAFs phosphorylation depends on ABP1/TMK1 and/or AFB1. Therefore, we arrayed  
353 all phosphosites in AtMARK's and compared their phosphorylation state in the mutant  
354 backgrounds (Figure 5C). In this analysis it is clear that MARK/RAF phosphorylation is  
355 strongly disturbed in each mutant, and that the *afb1* pattern more closely resembles that of  
356 wild-type, whereas *abp1* and *tmk1* more severely disturb MARK/RAF phosphorylation  
357 (Figure 5C). Interestingly, consistent with global patterns of the entire phosphoproteome  
358 (Roosjen, Kuhn et al, accompanying manuscript), for some MARK/RAF sites,  
359 phosphorylation is antagonistically distorted between *afb1* mutants and *abp1* and *tmk1*  
360 mutants.

361

## 362 **MARK links rapid phospho-response to fast auxin responses**

363

364 MARK/RAF proteins are a unique family of kinases that carry an N- terminal Phox-Bem1  
365 domain (PB1)<sup>63</sup> in addition to their C-terminal kinase domain (Figure 3B). PB1 domains can  
366 either mediate heterotypic or homotypic protein interaction with other PB1 domains, which  
367 can assemble into dimers or oligomers<sup>64,65</sup>. Apart from a single *Arabidopsis* paralog  
368 (HCR1)<sup>57</sup>, MARK/RAF protein localization has not been studied. We therefore generated  
369 translational fusions of *Arabidopsis* and *Marchantia* MARK/RAF proteins to fluorescent  
370 proteins and determined their localization. In both species, MARK/RAF proteins localized to  
371 punctate structures (Figure 6A, B) resembling the “punctae” observed for other PB1-  
372 containing proteins<sup>66-68</sup>. In both *Arabidopsis* roots (Figure 6A) and *Marchantia* gemmae  
373 (Figure 6B), these structures were associated both with the plasma membrane and in the  
374 cytoplasm. Thus, MARK/RAF protein locates to sites where fast auxin responses occur.

375        Given the profound role of MARK/RAF in mediating fast auxin-triggered  
376 phosphorylation changes, we explored whether MARK/RAF might mediate the rapid effect of  
377 auxin on membrane potential and cytoplasmic streaming. Responses to auxin treatment in  
378 membrane depolarization were normal in *mark* mutants in both *Arabidopsis* and *Marchantia*  
379 (Figure 6C, Supplementary Figure 4). However, we did find that *Arabidopsis mark/raf*  
380 mutants showed an altered apoplastic root surface pH profile (Supplementary Figure 5),  
381 perhaps caused by altered developmental zonation. Nonetheless, MARK/RAF does not appear  
382 to mediate auxin-triggered membrane depolarization (Figure 6C, Supplementary Figure 4)  
383 and the root surface alkalinization response (Supplementary Figure 5).

384        In contrast, already in untreated *Arabidopsis mark/raf* mutant root epidermal cells,  
385 cytoplasmic streaming is significantly reduced (Figure 6D; compare with Figure 2B).  
386 Interestingly, *mark/raf* mutants are essentially insensitive to the promoting effect of auxin in  
387 cytoplasmic streaming (Figure 6D). In *Marchantia* rhizoid cells, *mark/praf* mutants showed  
388 wild-type cytoplasmic streaming in untreated conditions, but like in *Arabidopsis*, mutant cells  
389 were insensitive to the promoting effect of auxin (Figure 6D; compare with Figure 2B). This  
390 suggests that MARK proteins have a conserved role in mediating auxin-promoted cytoplasmic  
391 streaming in *Arabidopsis* and *Marchantia*. Collectively, we conclude that MARK proteins link  
392 rapid phosphorylation changes to a fast cellular response to auxin.

393

394

395

396 **DISCUSSION**

397 Over the past decades, there have been impressive advances in understanding how auxin is  
398 synthesized, transported and degraded, and how it controls plant growth and development by  
399 regulating gene expression<sup>37</sup>. There are however several major open questions. Firstly: there  
400 is a number of auxin responses that are too rapid to be mediated by gene regulation, for which  
401 there is no mechanism yet. Secondly, no known mechanism can account for responses to  
402 auxin in algae, that lack the well-known transcriptional auxin response system<sup>11</sup>. In the  
403 accompanying article (Roosjen, Kuhn et al., accompanying manuscript) we identify a fast,  
404 unknown and unsuspected branch of auxin activity based on rapid protein phosphorylation, in  
405 Arabidopsis roots. Here, we demonstrate that this pathway is conserved across the green  
406 lineage, extending beyond land plants into the streptophyte algae. We show that some fast  
407 cellular responses to auxin are also conserved across land plants and algae and identify a key  
408 protein kinase mediating both auxin-triggered phosphorylation and a rapid cellular response.  
409 This identifies rapid phosphorylation-dependent signaling as a mechanism that can account  
410 for both fast and deeply conserved auxin responses.

411 Although we compared phosphoproteomes in different tissue types, and in both  
412 sporophytic (for Arabidopsis) and gametophytic tissue (for all other species), we detected a  
413 core set of functions and orthologous protein groups that are shared between all. The most  
414 parsimonious explanation is that this core set represents a truly ancient auxin “regulome” that  
415 has been retained in all these species to serve core functions. This is not trivial, given the  
416 estimated divergence times of between 850-500 Mya. In addition to the core set, there are  
417 numerous lineage/clade/group/organism-specific targets. This suggests profound  
418 diversification and neo-functionalization of auxin-triggered phosphorylation pathways. We  
419 have compiled all phosphoproteomics data generated in this study in the AuxPhos webtool  
420 (<https://weijerslab.shinyapps.io/AuxPhos>; Roosjen, Kuhn et al., accompanying manuscript),  
421 to allow facile access.

422 Though mining both comparative phosphoproteomics, kinase-substrate inference from  
423 temporal series and motif analysis, we identified a family of B4 RAF-like kinases  
424 (MARK/RAFs). Exploring mutants in orthologous proteins in Arabidopsis and Marchantia,  
425 we could establish that MARK/RAF kinases are central to auxin-triggered phosphorylation,  
426 and to development and physiological and cellular auxin response. Curiously, transcriptional  
427 auxin responses are not impaired, which suggests that the rapid, phosphorylation-based

428 pathway is mechanistically uncoupled from the nuclear auxin pathway. The mutants, even in  
429 the absence of auxin treatment, have dramatic phenotypes. It should however be kept in mind  
430 that members of the MARK/RAF family have been implicated in responses to other triggers  
431 (e.g. light, osmotic stress)<sup>57-59</sup>. Disruption of these responses likely also contribute to the  
432 strong phenotypes, and dedicated strategies will be required to deconvolute these roles.

433 Notably, regulation of most kinases that are differentially phosphorylated upon auxin  
434 treatment in wild-type *Marchantia* and *Arabidopsis*, is lost in *mark* mutants, suggesting that  
435 MARK/RAF may sit at the apex of a multi-tier phosphorylation network. Interestingly, RAF  
436 kinases, MARK/RAF orthologs in mammals, play an important role as master regulator of  
437 signaling cascades, for example in EGF signaling<sup>65</sup>. MARK phosphorylation upon auxin  
438 treatment occurs within 30 seconds in *Arabidopsis* (the earliest sampled timepoint; Roosjen,  
439 Kuhn et al., accompanying manuscript). Mammalian RAF kinases can be activated by  
440 phosphorylation within seconds to minutes after signal recognition<sup>69,70</sup>. Therefore, the kinetics  
441 of MARK/RAF activation is consistent with the phospho-activation of their orthologs in  
442 animal cells.

443 Mammalian RAF Kinases polymerize through their PB1 domain and localize in  
444 punctate structures in the cytoplasm to form so-called signalosomes<sup>65,68</sup>. Signalosomes are  
445 large supramolecular protein complexes that help increase avidity between signaling  
446 components. The formation of such signaling hubs and their association with receptors is  
447 crucial for signal transduction in some pathways<sup>64</sup>. Curiously, both *Arabidopsis* and  
448 *Marchantia* MARK/RAF proteins localize to punctate structures in the cytoplasm and at the  
449 plasma membrane. It will be interesting to see if these punctae are functional signalosomes,  
450 whether they form through PB1 domain oligomerization, and what other proteins they bring  
451 together.

452 Inspired by the finding that algae and land plants share a common set of auxin  
453 phosphotargets, we explored if there are also shared cellular and physiological responses.  
454 Indeed, cytoplasmic streaming is deeply conserved responses across land plants while  
455 membrane depolarization is deeply conserved across land plants and algae. Both are  
456 widespread cellular phenomena that are connected to for example cellular growth, nutrient  
457 distribution and acquisition<sup>50,71,72</sup>. It is not clear what function the auxin-regulation of these  
458 processes serves, but analysis of these responses in *mark/raf* mutants did help to show  
459 bifurcation of rapid auxin response mechanisms. While auxin-dependent acceleration of  
460 cytoplasmic streaming depended on MARK/RAF, membrane depolarization did not.

461 Interestingly, *mark/raf* mutants already had lower streaming velocity in the absence of auxin  
462 treatment, suggesting the same pathway operates during normal development, likely  
463 mediating the response to endogenous auxin.

464 The differential roles of MARK/RAF in the regulation of cytoplasmic streaming and  
465 membrane polarity are conserved between *Arabidopsis* and *Marchantia*, suggesting a deep  
466 evolutionary split between these two functions. In *Arabidopsis*, auxin-triggered membrane  
467 depolarization was previously attributed to the cytoplasmic AFB1 auxin receptor<sup>17</sup>, but its  
468 mechanism of action is not yet clear. Interestingly, AFB1 is a late innovation specific to  
469 angiosperms, and auxin-triggered membrane depolarization is found in the alga  
470 *Klebsormidium* that does not carry any TIR1/AFB ortholog<sup>11</sup>. This raises the question how  
471 the auxin signal translates to membrane depolarization outside of the angiosperms. Apart of  
472 the MARK/RAF-family, we identified B3-clade RAF-like kinases and PHOT1 kinases as  
473 potential conserved hubs in the auxin phosphorylation. It will be interesting to see if these  
474 kinases play a role in regulating membrane depolarization. Interestingly, PHOT1 was  
475 previously shown to mediate a rapid blue light-triggered membrane depolarization in  
476 *Arabidopsis*<sup>73</sup>, making it a strong candidate.

477 A key question is how the auxin signal is perceived and transmitted onto MARK/RAF  
478 proteins, given that MARK/RAFs do not have a clear ligand-binding domain. The auxin  
479 response components ABP1, TMK1 and AFB1 all contribute to auxin-triggered  
480 phosphorylation changes in *Arabidopsis* (Roosjen, Kuhn et al., accompanying manuscript).  
481 MARK/RAF phosphorylation was disturbed in all three mutants, but is clear from global  
482 phosphoproteomes that the response is not linear, and likely relatively complex. MARK/RAF  
483 kinases now offer a strong starting point to mechanistically dissect the response pathway,  
484 including its receptor. It is encouraging that ABP1 is deeply conserved among land plants and  
485 algae (Supplementary Figure 6). While no clear ortholog is present in *Marchantia*<sup>74</sup>, ABP1 is  
486 member of the large Cupin family, and other members of this family in *Arabidopsis* also  
487 appear to function as auxin receptors<sup>75</sup> co-submitted manuscript. This raises the interesting possibility  
488 that the broader Cupin family, represented in all domains of life<sup>76</sup>, may act as auxin receptors  
489 for fast responses, including those mediated by MARK/RAF.

490 One striking aspect of the phosphorylation response we have discovered, is that it  
491 clearly predates the origin of the nuclear auxin response pathway<sup>11</sup>. Thus, well before the  
492 innovations appeared that led to auxin-dependent gene regulation, algal cells possessed a

493 system to rapidly respond to auxin. The nuclear auxin response did not evolve to replace this  
494 system, as the rapid response system has been retained in land plants. Thus, the rapid system  
495 likely regulates responses that the nuclear system cannot, and vice versa. This could in part  
496 reflect the fundamental difference in auxin controlling cellular physiology and cell identity  
497 and fate, which happen at very different timescales. The description of this response and its  
498 deep origin, and the identification of the first component, now opens avenues to genetically  
499 and biochemically characterize these pathways in the future. This will likely deepen our  
500 understanding on the origins of auxin signaling and help reveal the ancestral role of auxin  
501 within the green lineage.

502

503

504 **ACKNOWLEDGEMENTS**

505

506 We are grateful to Asuka Shitaku and Eri Koide for generating and sharing the Marchantia  
507 MARK/PRAF-mCitrine line, to Peng-Cheng Wang for sharing the Arabidopsis mark/raf  
508 mutants, and to our team members for discussions and helpful advice. This work was  
509 supported by funding from the Netherlands Organization for Scientific Research (NWO):  
510 VICI grant 865.14.001 and ENW-KLEIN OCENW.KLEIN.027 grants to D.W. and VENI  
511 grant VI.VENI.212.003 to A.K.; the European Research Council AdG DIRNDL (contract  
512 number 833867) to D.W., CoG CATCH to J.S., StG CELLONGATE (contract 803048) to  
513 M.F. and AdG ETAP (contract 742985) to J.F.; MEXT KAKENHI Grant number  
514 JP19H05675 to T.K.; JSPS KAKENHI Grant Number JP20H03275 to R.N., Takeda Science  
515 Foundation to R.N.; the VLAG graduate school to M.v.G. and the Austrian Science Fund  
516 (FWF, P29988) to J.F..

517

518 **AUTHOR CONTRIBUTIONS,**

519

520 Conceptualization: A.K., M.R., D.W.; Methodology: A.K., M.R., P.C.C., S.M., S.M.D., J.S.;  
521 Formal analysis: M.R., A.K., P.C.C., S.M., S.M.D., A.M., M.F., J.S.; Investigation: A.K.,  
522 M.R., P.C.C., S.M., S.M.D., A.M.; Resources: R.N., T.K.; Writing – Original Draft: A.K.,  
523 D.W.; Writing – Review & Editing: all authors; Visualization: A.K., M.R., P.C.C., S.M.,  
524 S.M.D.; Supervision: M.F., J.F., J.S., D.W.; Funding Acquisition: A.K., M.F., J.F., J.S., D.W..

525

526

527

528 **DECLARATION OF INTERESTS**

529

530 None of the authors have competing interest to declare.

531

532

533

534 **MATERIALS AND METHODS**

535

536 **Plant material and culture conditions**

537 All plants were cultured under 90-100  $\mu\text{mol}$  photons  $\text{m}^{-2} \text{ s}^{-1}$  white light with a 16 h light / 8  
538 dark cycle at 22 °C and 75% humidity. *Arabidopsis thaliana* wild type Columbia-0 (Col-0)  
539 and all *Arabidopsis* mutants and transgenics were cultured on half strength Murashige and  
540 Skoog (MS) basal medium <sup>77</sup> at pH 5.7 supplemented with 0.8 % agar. All *Arabidopsis*  
541 mutants use were previously published: *tmk1-1* (SALK\_016360) <sup>78</sup>, *abp1-td1* <sup>79</sup>, *afb1-3* <sup>80</sup>,  
542 *mark/raf<sup>null</sup>* (published as OK<sup>130null</sup>) <sup>58</sup> and *mark/raf<sup>weak</sup>* (published as OK<sup>130weak</sup>) <sup>58</sup>.

543 *Marchantia polymorpha* wild type strain Takaragaike-1 (Tak-1) and all *Marchantia*  
544 mutants and transgenics were cultured on half strength Gamborg's B5 medium (B5 medium,  
545 <sup>81</sup>) pH 5.7 supplemented with 1% agar. The *Marchantia* *mark/praf<sup>ko</sup>* mutant was previously  
546 published as *Mppraf<sup>ko</sup>* <sup>59</sup>.

547 *Klebsormidium nitens* (NIES-2285) and *Physcomitrium patens* (Gransden strain) was  
548 cultured on BCD medium <sup>82</sup> supplemented with 1 % agar under the same condition as *M.*  
549 *polymorpha*. *Penium margaritaceum* was cultured in liquid Woods Hole medium <sup>83</sup> at pH 7.2  
550 under gentle agitation (60RPM) at 20°C with a 16 h light / 8 dark cycle, 30 – 50  $\mu\text{mol}$   
551 photons  $\text{m}^{-2} \text{ s}^{-1}$  light in 50 ml Erlenmeyer flasks.

552

553 **Phosphoproteomics**

554 Treatment for phosphoproteomics was carried out as described in (Roosjen, Kuhn et al.,  
555 accompanying manuscript) with the following adjustments: *Klebsormidium nitens*,  
556 *Physcomitrium patens* and *Marchantia polymorpha* were grown for 10 days on plates as  
557 described above, then treated with 100 nM IAA or DMSO in the respective growth medium  
558 for 2 minutes, harvested and frozen in liquid nitrogen. *Penium margaritaceum* was grown for  
559 15 days as described above. Cells were collected by centrifugation at 1620 g for 2 min and  
560 washed 3 times with 10 ml of WHM to remove any residual extracellular polysaccharides  
561 from the cell surface. The pellet was resuspended in 10 ml of media and cells were treated  
562 with 100 nM IAA or DMSO for 2 min, harvested by centrifugation at 1620 g for 2 min and  
563 frozen in liquid nitrogen. Sample preparation and data analysis was carried out as described in  
564 (Roosjen, Kuhn et al., accompanying manuscript) with the following adjustments: for  
565 *Marchantia polymorpha* the UP000244005 proteome was used, for *Physcomitrium patens* the  
566 UP000006727 proteome was used, for *Klebsormidium nitens* the UP000054558 proteome was  
567 used and for *Penium margaritaceum* the proteome from a whole genome assembly was used

568 <sup>48</sup>. The mass spectrometry proteomics data, protein lists and intensity values of all samples  
569 have been deposited to the ProteomeXchange Consortium via the PRIDE <sup>84</sup> partner repository  
570 with the dataset identifier XXX. All phosphoproteomics data has been compiled in the  
571 AuxPhos web-app (<https://weijerslab.shinyapps.io/AuxPhos>; Roosjen, Kuhn et al.,  
572 accompanying manuscript).

573

#### 574 **Orthogroup construction**

575 Identification of orthogroups i.e., common orthologous sequences between multiple species  
576 were estimated using Orthofinder <sup>85</sup>. Proteomes used for this analysis include: *Arabidopsis*  
577 *thaliana* (Araport11), *Marchantia polymorpha* (v6.1), *Physcomitrium patens* (v3.3),  
578 *Klebsormidium nitens* (v1.1) and *Penium margaritaceum* (v1).

579

#### 580 **Cytoplasmic streaming**

581 Cytoplasmic streaming was recorded using a Leica SP5 or SP8 confocal microscope equipped  
582 with HyD detectors using Apo  $\lambda$  63 $\times$ /1.10 water immersion objective plus 6x digital zoom in  
583 an 256x256 pixel format. Cytoplasmic streaming was recorded and analyzed for *Arabidopsis*  
584 epidermal cells of the root elongation zone and *Marchantia* rhizoid cells using the following  
585 method: Seven day old *Arabidopsis* plate-grown seedlings were taken into the microscopy  
586 room and mitochondria were stained by transferring the seedling into a petri dish with liquid  
587  $\frac{1}{2}$  MS medium containing 1  $\mu$ M Rhodamine 123 for 5 minutes. Subsequently, seedlings were  
588 washed with liquid  $\frac{1}{2}$  MS without Rhodamine 123. Seedlings were then transferred to  
589 microscopy slides in a drop of liquid  $\frac{1}{2}$  MS containing 100 nM IAA or DMSO, covered by a  
590 coverslip and left on the microscope stage to adapt to the environment for 30 minutes.  
591 Cytoplasmic streaming was recorded in at least 5 epidermal cells of the root elongation zone  
592 per root at a frame rate of 5.3 frames per second for 30 seconds (159 frames).

593 Prior to the experiment, *Marchantia* thallus was grown from gemmae for two days in  
594 liquid B5 medium in a petridish. After two days of cultivation Rhodamine 123 was added to a  
595 final concentration of 1  $\mu$ M and Triton-X-100 was added to a final concentration of 0.01%.  
596 *Marchantia* samples were stained for 30 minutes and then washed three time with liquid B5  
597 medium containing 0.01% Triton-X-100 without Rhodamine 123. Samples were then  
598 transferred to microscopy slides and cytoplasmic streaming in rhizoid cells was recorded as  
599 described for *Arabidopsis*.

600

#### 601 **Data analysis for cytoplasmic streaming**

602 Data analysis was performed in MatLab (version: 2021b). First, static background signal was  
603 removed from the raw fluorescence images using a moving window median filter (averaging  
604 window = 25 frames) and motile objects smoothed with a 2-pixel Gaussian blur filter. Moving  
605 objects were tracked using an established particle tracking algorithm <sup>86</sup>, keeping only those  
606 trajectories whose length exceeds 3 seconds. For each cell, from the individual trajectories of  
607 the remaining moving objects, typically between 30 to 60 per time series, an ensemble-  
608 averaged mean-squared displacement was computed:

609

$$\Delta r^2(\tau) = \langle |r(t + \tau) - r(t)|^2 \rangle$$

610

611 Per cell, these mean-squared displacements were fitted to the anomalous diffusion model  
612 (ADM) <sup>87,88</sup>, a generalization of Einstein's diffusion model to describe complex non-Fickian  
613 motion of organelles in the visco-elastic liquid of the cellular cytosol, which is composed of  
614 an unknown mixture of passive (Brownian) and active (streaming) transport in a crowded and  
615 heterogeneous medium:

616

$$\Delta r^2(\tau) = K\tau^\alpha$$

617

618 where  $\tau$  is the correlation time. In the ADM, the generalized diffusion power law exponent  $\alpha$   
619 provides information on the average nature of the transport processes:  $\alpha < 1$  is indicative of  
620 sub-diffusive motion, characteristic of Brownian motion in a visco-elastic liquid,  $\alpha = 1$   
621 indicates pure Brownian motion in a viscous liquid and  $\alpha > 1$ , known as super-diffusion,  
622 indicates transport with an active, e.g., motor-protein driven, component. Intermediate values  
623 of the power law exponent  $\alpha$  provide insight into the relative balance of these different  
624 processes on the organellar motion. The transport rate constant  $K$  (in units mm/s<sup>3</sup>) informs  
625 about the average transport rate: the larger the value of  $K$  the faster the organellar transport in  
626 the cells. Our analysis yields one average value for  $\alpha$  and  $K$  per cell; the significance of the  
627 differences between control and treatment was assessed with a two-sided Wilcoxon signed  
628 rank test.

629

### 630 **Membrane potential measurement using DISBAC<sub>2</sub>(3)**

631 Membrane potential was measured using the DISBAC<sub>2</sub>(3) probe as previously described for  
632 *Arabidopsis*<sup>17</sup>. DISBAC<sub>2</sub>(3) (2  $\mu$ M) was added to buffered ½ MS liquid medium with 1%

633 (w/v) sucrose containing either 0 or 100 nM IAA. Five-day-old *Arabidopsis* seedlings were  
634 transferred to a sealable single-layer PDMS silicone chip<sup>17</sup>. The PDMS silicone chip  
635 containing the seedlings was then placed on a vertical spinning disk microscope for a 20-min  
636 recovery. During the recovery process, the seedlings were treated with control medium at a  
637 flow rate of 3  $\mu$ l/min. Seedlings were imaged every 30 seconds with a x20/0.8 objective.  
638 DISBAC2(3) was excited with a 515-nm laser, and the emission was filtered with a 535/30-  
639 nm bandpass filter. DISBAC2(3) fluorescence was measured at the border between epidermis  
640 and cortical cells of the transition zone by selecting 5-6 or 3-4 cells for *Col-0* and  
641 *Atmark/raf<sup>null</sup>*, respectively.

642 Membrane potential of *Marchantia* and *Klebsormidium* was measured using the same  
643 probe with the following modifications to the protocol: *Marchantia* gemmae were removed  
644 from gemmae cups and placed liquid B5 with 0.01% Triton-X-100 supplemented with 15  $\mu$ M  
645 DISBAC<sub>2</sub>(3), vacuum infiltrated for 5 minutes and transferred to a cover slip followed by  
646 incubation for 30 minutes before imaging. Imaging was performed on an inverted Leica SP8  
647 confocal microscope using the same setting as for *Arabidopsis*. *Klebsormidium* was grown for  
648 10 days as described above. A small amount of *Klebsormidium* was then scraped off the plate  
649 and dissolved in liquid BCD medium supplemented with 15  $\mu$ M DISBAC<sub>2</sub>(3) followed by  
650 incubation for 30 minutes before imaging.

651

## 652 **Root surface pH profile**

653 Root surface pH was measured using the ratiometric Fluorescein-5-(and-6)-Sulfonic Acid,  
654 Trisodium Salt (FS) (Invitrogen<sup>TM</sup> F1130)<sup>89</sup>. Five-day-old *Arabidopsis* seedlings were  
655 transferred to unbuffered 1/2 MS medium containing 50  $\mu$ M FS dye and either 0 or 100 nM  
656 IAA. Seedlings were allowed to recover on a vertical spinning disk microscope for 20 minutes  
657 after transfer to the microscope chamber. Imaging was performed using a vertical stage Zeiss  
658 Axio Observer 7 microscope coupled to a Yokogawa CSU-W1-T2 spinning disk unit with 50  
659  $\mu$ m pinholes, equipped with a VS-HOM1000 excitation light homogenizer (Visitron  
660 Systems). Images were acquired using VisiView software (Visitron Systems, v.4.4.0.14). We  
661 used a Zeiss Plan-Apochromat  $\times 10/0.45$  objective. FS was excited by 405 and 488 nm laser.  
662 The 488/405 nm fluorescence emission ratio along the root was calculated using the ATR  
663 software<sup>89</sup>.

664

## 665 **Phenotyping**

666 Arabidopsis ***plant height*** was determined from respectively 48 individual wild type and  
667 *mark/raf<sup>null</sup>* senescent plants, seven weeks after germination. To compare the ***leaf area*** of  
668 fully elongated leaf 6 to leaf 9 of Arabidopsis wild type, *mark/raf<sup>null</sup>* and *mark/raf<sup>weak</sup>*, 16  
669 plants per genotype were collected, flattened on paper and photographed using a Canon EOS  
670 250D with EFS 18-135mm Macro Lens. Leaf area was measured in ImageJ (Version 1.52)  
671 using the Polygon selection tool.

672 ***Rosette area*** was determined from respectively 90 individual wild type and *mark/raf<sup>null</sup>* plants  
673 plants 28 days after germination. Plants were photographed individually using a Canon EOS  
674 250D camera with EFS 18-135mm Macro Lens. Rosette area was then measured in ImageJ  
675 (Version 1.52) using the Polygon selection tool. To compare the ***germination efficiency***  
676 between *mark/raf<sup>null</sup>* mutants and wild type, seeds for each genotype were surface sterilized,  
677 stratified in a 0.1% agarose solution for two days at 4 °C and placed on half strength MS plates  
678 (0.8% Agar). Plates were grown vertically for 9 days and germinated seeds were scored at day  
679 1, 2, 3, 4, 7 and 9. Germination percentages were calculated for each day. The experiment was  
680 repeated three times individually and data were combined for analysis.

681 Seedlings of Arabidopsis wild type, *mark/raf<sup>null</sup>* and *mark/raf<sup>weak</sup>* were germinated on half  
682 strength MS and vertically grown for 5 days. After five days, ten seedlings with representative  
683 root length for each genotype were transferred to new square petri dishes either containing 1  
684 nM IAA, 100 nM IAA or a mock treatment representing an equal amount of solvent (DMSO).  
685 ***Root length*** was captured by photographing the plates immediately after transferring the  
686 seedlings, after 24 hour, after 48 hours and after 120 hours, using a Canon EOS 250D camera  
687 with EFS 18-135mm Macro Lens. Root length was then measured in ImageJ using the  
688 segmented line tool and growth rates calculated.

689 To compare the ***thallus growth*** between *Marchantia mark/praf<sup>ko</sup>* mutants (n=44) and  
690 wild type (n=50), thalli were grown from gemmae on half strength Gamborg B5 medium.  
691 Plates were grown for 29 days and projected thallus area was captured by photographing the  
692 plates immediately after transferring the gemmae, after 2, 4, 7, 9, 11, 14, 16, 18, 22 and 29  
693 days, using a Canon EOS 250D camera with EFS 18-135mm Macro Lens. Thallus area was  
694 then measured in ImageJ (Version 1.52) using the Polygon selection tool. For ***auxin***  
695 ***sensitivity*** assays, *Marchantia mark/praf<sup>ko</sup>* mutant (n=10) or wild-type (n=10) gemmae were  
696 grown on half strength Gamborg B5 medium supplemented the indicated concentration of  
697 IAA and grown for 10 days. At day 10, thallus size was captured by photographing the plates  
698 using a Canon EOS 250D with EFS 18-135mm Macro Lens. Thallus area was then measured  
699 in ImageJ (Version 1.52) using the Polygon selection tool. ***Gemma cup number*** was

700 determined on *mark/praf*<sup>ko</sup> mutants (n=14) and wild type (n=14) thalli after 24 days of growth  
701 on half strength Gamborg B5 medium.

702

### 703 Transcriptomic analysis

704 *Arabidopsis thaliana* wild-type (Col-0) and mutant (*mark/raf*<sup>null</sup>) seeds were sown on half-  
705 strength MS medium covered with nylon mesh and vertically grown for 7 days. Plants were  
706 then submerged in liquid half-strength MS medium containing either 1 µM IAA or the  
707 equivalent amount of solvent (DMSO). Plates were kept horizontally for about 30 seconds  
708 and then kept vertically for 1 hour to incubate. After incubation, root tips were harvested  
709 using a scalpel and immediately frozen in liquid nitrogen.

710 *Marchantia polymorpha* wild-type (Tak-1) and mutant (*mark/praf*<sup>ko</sup>) gemmae were  
711 placed on B5 solid medium covered with nylon mesh (100 mm pore) and grown for 9 days.  
712 After growing, plants were submerged in liquid B5 medium and cultured for 1 day. After pre-  
713 cultivation, IAA was added to a final concentration of 1 µM or an equivalent amount of  
714 DMSO was added and plants were incubated for 1 hour. Using a scalpel, thalli were harvested  
715 from the mesh, blotted on paper towels and immediately frozen in liquid nitrogen.

716 After harvesting, all frozen samples were ground into fine powder using a pre-cooled  
717 mortar and pestle. Total RNA from all samples was extracted using a RNeasy Plant Mini Kit  
718 (QIAGEN). Total RNA was treated with RNase-free DNase I set (QIAGEN). RNA-seq  
719 library construction and RNA sequencing were performed by BGI Tech Solutions (Hong  
720 Kong).

721

### 722 RNAseq data analysis

723 Up to 20 million paired-end 150 bp reads were collected for each sample. Quality assessment  
724 for raw reads was performed using FastQC  
725 ([www.bioinformatics.babraham.ac.uk/projects/fastqc](http://www.bioinformatics.babraham.ac.uk/projects/fastqc)). For both *Arabidopsis thaliana*  
726 (Araport11; <sup>90</sup>) and *Marchantia polymorpha* (v6.1; <sup>91</sup>), reads were mapped onto the  
727 respective genomes using HISAT2 (v2.1.0; <sup>92</sup>) with additional parameters “--trim5 10 -dta”.  
728 Alignment (SAM/BAM) files were sorted and indexed using SAMTOOLS (v1.9; <sup>93</sup>).  
729 FeatureCounts (v2.0.0; <sup>94</sup>) was used to count the reads mapped on to each gene, with the  
730 parameters “-t 'exon' -g 'gene\_id' -Q 30 --primary -p -B -C” for *Arabidopsis* transcripts and “t  
731 'gene' -g 'ID' -Q 30 --primary -p -B -C” for *Marchantia* transcripts. DEseq2 <sup>95</sup> was used to  
732 normalize the raw counts and perform the differential expression analysis with a design  
733 matrix including the interaction term (Padj<0.05). Data processing and statistical analysis was

734 performed using R (<https://www.r-project.org/>). Sequenced raw reads were deposited in NCBI  
735 Sequence Read Archive (SRA) under the project accession number PRJNA881051.

736

737 **Generation of transgenics**

738 Primers used in this study can be found in Supplementary Table 1. *Arabidopsis* MARK  
739 reporter lines for MARK1/RAF24 and MARK5/RAF20 under their endogenous promoter  
740 were generated by amplifying the genomic fragment including the 3.5 kb region upstream of  
741 the start codon using the appropriate primers for each gene. Fragments were cloned into a  
742 pGIIK LIC-YFP (pPLV17) vector<sup>96</sup> using the HiFi cloning kit (ThermoFisher).

743 For the *Marchantia* MARK/PRAF reporter line, a DNA fragment for an *Arabidopsis*-  
744 codon-optimized mCitrine coding sequence (CDS) was synthesized (IDT) and used to amplify  
745 a GGS $\square$ 2 linker-containing fragment by PCR with a primer set,  
746 pUGW2\_Aor\_GGS2\_mCit\_IF\_F and pUGW2\_Aor\_mCit\_IF\_R, which was then cloned into  
747 the Aor51HI site in pUGW2 35S<sup>97</sup> using the In-Fusion cloning kit (TaKaRa Bio). The 2.5-kb  
748 HindIII-SacI fragment in the resulting plasmid, including the Gateway cassette followed by  
749 the GGS $\square$ 2 linker-attached mCitrine CDS, was ligated with the HindIII- and SacI-digested  
750 pMpGWBx00<sup>97</sup> to generate pMpGWBx47. The MpMARK/PRAF genomic sequence  
751 covering its promoter and CDS (without stop codon) in pENTR/D-TOPO\_MpMARK/PRAF  
752<sup>59</sup> was transferred to pMpGWB347 to generate pMpGWB347-MpMARK/PRAF.  
753 Agrobacterium GV2260 containing pMpGWB347-MpMARK/PRAF was used to transform  
754 Mpmark/praf<sup>ko</sup> plants (Koide et al. 2020) by the thallus transformation method<sup>98</sup>.

755

756 **Imaging of transgenic lines plants for MARK-localization analysis:**

757 *Marchantia* gemmae expressing MARK/PRAF-mCitrine under endogenous promoter and 7  
758 day-old *Arabidopsis* roots expressing MARK1/RAF24-YFP or MARK5/RAF20-YFP under  
759 their respective endogenous promoter were imaged using a Leica SP5 or SP8 confocal  
760 microscope equipped with an Argon laser (SP5) or a white light laser (SP8). Both, mCitrine  
761 and YFP were excited at 514 nm, and emission was collected between 525-575 nm. Images  
762 were analyzed using ImageJ (Version 1.52).

763

764 **REFERENCES**

765

- 766 1. Friml, J. (2022). Fourteen Stations of Auxin. *Cold Spring Harb Perspect Biol* **14**,  
767 a039859. [10.1101/cshperspect.a039859](https://doi.org/10.1101/cshperspect.a039859).
- 768 2. Friml, J., Wiśniewska, J., Benková, E., Mendgen, K., and Palme, K. (2002). Lateral  
769 relocation of auxin efflux regulator PIN3 mediates tropism in *Arabidopsis*. *Nature* **415**,  
770 806–809. [10.1038/415806a](https://doi.org/10.1038/415806a).
- 771 3. Tao, Y., Ferrer, J.-L., Ljung, K., Pojer, F., Hong, F., Long, J.A., Li, L., Moreno, J.E.,  
772 Bowman, M.E., Ivans, L.J., et al. (2008). Rapid Synthesis of Auxin via a New  
773 Tryptophan-Dependent Pathway Is Required for Shade Avoidance in Plants. *Cell* **133**,  
774 164–176. [10.1016/j.cell.2008.01.049](https://doi.org/10.1016/j.cell.2008.01.049).
- 775 4. Went, F.W., and Thimann, K.V. (1937). *Phytohormones* (MacMillan Company).
- 776 5. Went, F.W. (1928). *Wuchsstoff und Wachstum. Recueil des travaux botaniques*  
777 *néerlandais* **25**, 1–116.
- 778 6. Sessions, R.A., and Zambryski, P.C. (1995). *Arabidopsis* gynoecium structure in the  
779 wild and in ettin mutants. *Development* **121**, 1519–1532. [10.1242/dev.121.5.1519](https://doi.org/10.1242/dev.121.5.1519).
- 780 7. Nemhauser, J.L., Feldman, L.J., and Zambryski, P.C. (2000). Auxin and ETTIN in  
781 *Arabidopsis* gynoecium morphogenesis. *Development* **127**, 3877–3888.  
782 [10.1242/dev.127.18.3877](https://doi.org/10.1242/dev.127.18.3877).
- 783 8. Scarpella, E., Marcos, D., Friml, J., and Berleth, T. (2006). Control of leaf vascular  
784 patterning by polar auxin transport. *Genes Dev* **20**, 1015–1027. [10.1101/gad.1402406](https://doi.org/10.1101/gad.1402406).
- 785 9. de Rybel, B., Adibi, M., Breda, A.S., Wendrich, J.R., Smit, M.E., Novák, O., Yamaguchi,  
786 N., Yoshida, S., van Isterdael, G., Palovaara, J., et al. (2014). Integration of growth and  
787 patterning during vascular tissue formation in *Arabidopsis*. *Science* (1979) **345**,  
788 [10.1126/science.1255215](https://doi.org/10.1126/science.1255215).
- 789 10. Morffy, N., and Strader, L.C. (2020). Old Town Roads: routes of auxin biosynthesis  
790 across kingdoms. *Curr Opin Plant Biol* **55**, 21–27. [10.1016/j.pbi.2020.02.002](https://doi.org/10.1016/j.pbi.2020.02.002).
- 791 11. Mutte, S.K., Kato, H., Rothfels, C., Melkonian, M., Wong, G.K.-S., and Weijers, D.  
792 (2018). Origin and evolution of the nuclear auxin response system. *Elife* **7**,  
793 [10.7554/elife.33399](https://doi.org/10.7554/elife.33399).
- 794 12. JIN, Q., SCHERP, P., HEIMANN, K., and HASENSTEIN, K. (2008). Auxin and cytoskeletal  
795 organization in algae. *Cell Biol Int* **32**, 542–545. [10.1016/j.cellbi.2007.11.005](https://doi.org/10.1016/j.cellbi.2007.11.005).
- 796 13. Park, W.-K., Yoo, G., Moon, M., Kim, C.W., Choi, Y.-E., and Yang, J.-W. (2013).  
797 Phytohormone Supplementation Significantly Increases Growth of *Chlamydomonas*  
798 *reinhardtii* Cultivated for Biodiesel Production. *Appl Biochem Biotechnol* **171**, 1128–  
799 1142. [10.1007/s12010-013-0386-9](https://doi.org/10.1007/s12010-013-0386-9).
- 800 14. Vance, B.D. (1987). Phytohormone effects on cell division in *Chlorella pyrenoidosa*  
801 chick (TX-7-11-05) (chlorellaceae). *J Plant Growth Regul* **5**, 169–173.  
802 [10.1007/BF02087185](https://doi.org/10.1007/BF02087185).
- 803 15. Etherton, B. (1970). Effect of Indole-3-acetic Acid on Membrane Potentials of Oat  
804 Coleoptile Cells. *Plant Physiol* **45**, 527–528. [10.1104/pp.45.4.527](https://doi.org/10.1104/pp.45.4.527).
- 805 16. Bates, G.W., and Goldsmith, M.H.M. (1983). Rapid response of the plasma-membrane  
806 potential in oat coleoptiles to auxin and other weak acids. *Planta* **159**, 231–237.  
807 [10.1007/BF00397530](https://doi.org/10.1007/BF00397530).

808 17. Serre, N.B.C., Kralík, D., Yun, P., Slouka, Z., Shabala, S., and Fendrych, M. (2021). AFB1  
809 controls rapid auxin signalling through membrane depolarization in *Arabidopsis*  
810 *thaliana* root. *Nat Plants* **7**, 1229–1238. 10.1038/s41477-021-00969-z.

811 18. Friml, J., Gallei, M., Gelová, Z., Johnson, A., Mazur, E., Monzer, A., Rodriguez, L.,  
812 Roosjen, M., Verstraeten, I., Živanović, B.D., et al. (2022). ABP1-TMK auxin perception  
813 for global phosphorylation and auxin canalization. *Nature* **609**, 575–581.  
814 10.1038/s41586-022-05187-x.

815 19. Ayling, S., and Clarkson, D. (1996). The Cytoplasmic Streaming Response of Tomato  
816 Root Hairs to Auxin; the Role of Calcium. *Functional Plant Biology* **23**, 699.  
817 10.1071/PP9960699.

818 20. Monshausen, G.B., Miller, N.D., Murphy, A.S., and Gilroy, S. (2011). Dynamics of auxin-  
819 dependent Ca<sup>2+</sup> and pH signaling in root growth revealed by integrating high-  
820 resolution imaging with automated computer vision-based analysis. *The Plant Journal*  
821 **65**, 309–318. 10.1111/j.1365-313X.2010.04423.x.

822 21. Barbez, E., Dünser, K., Gaidora, A., Lendl, T., and Busch, W. (2017). Auxin steers root  
823 cell expansion via apoplastic pH regulation in *Arabidopsis thaliana*. *Proceedings of the*  
824 *National Academy of Sciences* **114**. 10.1073/pnas.1613499114.

825 22. Shih, H.-W., DePew, C.L., Miller, N.D., and Monshausen, G.B. (2015). The Cyclic  
826 Nucleotide-Gated Channel CNGC14 Regulates Root Gravitropism in *Arabidopsis*  
827 *thaliana*. *Current Biology* **25**, 3119–3125. 10.1016/j.cub.2015.10.025.

828 23. Li, L., Verstraeten, I., Roosjen, M., Takahashi, K., Rodriguez, L., Merrin, J., Chen, J.,  
829 Shabala, L., Smet, W., Ren, H., et al. (2021). Cell surface and intracellular auxin  
830 signalling for H<sup>+</sup> fluxes in root growth. *Nature* **599**, 273–277. 10.1038/s41586-021-  
831 04037-6.

832 24. Senn, A.P., and Goldsmith, M.H.M. (1988). Regulation of Electrogenic Proton Pumping  
833 by Auxin and Fusicoccin as Related to the Growth of *Avena* Coleoptiles. *Plant Physiol*  
834 **88**, 131–138. 10.1104/pp.88.1.131.

835 25. Arieti, R.S., and Staiger, C.J. (2020). Auxin-induced actin cytoskeleton rearrangements  
836 require AUX1. *New Phytologist* **226**, 441–459. 10.1111/nph.16382.

837 26. Narasimhan, M., Gallei, M., Tan, S., Johnson, A., Verstraeten, I., Li, L., Rodriguez, L.,  
838 Han, H., Himschoot, E., Wang, R., et al. (2021). Systematic analysis of specific and  
839 nonspecific auxin effects on endocytosis and trafficking. *Plant Physiol* **186**, 1122–1142.  
840 10.1093/plphys/kiab134.

841 27. Heisler, M.G., Ohno, C., Das, P., Sieber, P., Reddy, G. v., Long, J.A., and Meyerowitz,  
842 E.M. (2005). Patterns of Auxin Transport and Gene Expression during Primordium  
843 Development Revealed by Live Imaging of the *Arabidopsis* Inflorescence Meristem.  
844 *Current Biology* **15**, 1899–1911. 10.1016/j.cub.2005.09.052.

845 28. Dubrovsky, J.G., Sauer, M., Napsucialy-Mendivil, S., Ivanchenko, M.G., Friml, J.,  
846 Shishkova, S., Celenza, J., and Benková, E. (2008). Auxin acts as a local morphogenetic  
847 trigger to specify lateral root founder cells. *Proceedings of the National Academy of*  
848 *Sciences* **105**, 8790–8794. 10.1073/pnas.0712307105.

849 29. Reinhardt, D., Pesce, E.-R., Stieger, P., Mandel, T., Baltensperger, K., Bennett, M.,  
850 Traas, J., Friml, J., and Kuhlemeier, C. (2003). Regulation of phyllotaxis by polar auxin  
851 transport. *Nature* **426**, 255–260. 10.1038/nature02081.

852 30. Thimann, K. v. (1938). HORMONES AND THE ANALYSIS OF GROWTH. *Plant Physiol* **13**,  
853 437–449. 10.1104/pp.13.3.437.

854 31. Hertel, R., Thomson, K.-St., and Russo, V.E.A. (1972). In-vitro auxin binding to  
855 particulate cell fractions from corn coleoptiles. *Planta* **107**, 325–340.  
856 10.1007/BF00386394.

857 32. Kepinski, S., and Leyser, O. (2005). The *Arabidopsis* F-box protein TIR1 is an auxin  
858 receptor. *Nature* **435**, 446–451. 10.1038/nature03542.

859 33. Dharmasiri, N., Dharmasiri, S., and Estelle, M. (2005). The F-box protein TIR1 is an  
860 auxin receptor. *Nature* **435**, 441–445. 10.1038/nature03543.

861 34. Tan, X., Calderon-Villalobos, L.I.A., Sharon, M., Zheng, C., Robinson, C. v., Estelle, M.,  
862 and Zheng, N. (2007). Mechanism of auxin perception by the TIR1 ubiquitin ligase.  
863 *Nature* **446**, 640–645. 10.1038/nature05731.

864 35. Gray, W.M., Kepinski, S., Rouse, D., Leyser, O., and Estelle, M. (2001). Auxin regulates  
865 SCFTIR1-dependent degradation of AUX/IAA proteins. *Nature* **414**, 271–276.  
866 10.1038/35104500.

867 36. Kim, J., Harter, K., and Theologis, A. (1997). Protein–protein interactions among the  
868 Aux/IAA proteins. *Proceedings of the National Academy of Sciences* **94**, 11786–  
869 11791. 10.1073/pnas.94.22.11786.

870 37. Weijers, D., and Wagner, D. (2016). Transcriptional Responses to the Auxin Hormone.  
871 *Annu Rev Plant Biol* **67**, 539–574. 10.1146/annurev-arplant-043015-112122.

872 38. Prigge, M.J., Platret, M., Kadakia, N., Zhang, Y., Greenham, K., Szutu, W., Pandey, B.K.,  
873 Bhosale, R.A., Bennett, M.J., Busch, W., et al. (2020). Genetic analysis of the  
874 *Arabidopsis* TIR1/AFB auxin receptors reveals both overlapping and specialized  
875 functions. *eLife* **9**. 10.7554/eLife.54740.

876 39. Hamann, T., Benkova, E., Bäurle, I., Kientz, M., and Jürgens, G. (2002). The *Arabidopsis*  
877 *BODENLOS* gene encodes an auxin response protein inhibiting MONOPTEROS-  
878 mediated embryo patterning. *Genes Dev* **16**, 1610–1615. 10.1101/gad.229402.

879 40. Hardtke, C.S., and Berleth, T. (1998). The *Arabidopsis* gene MONOPTEROS encodes a  
880 transcription factor mediating embryo axis formation and vascular development.  
881 *EMBO J* **17**, 1405–1411. <https://doi.org/10.1093/emboj/17.5.1405>.

882 41. Kato, H., Mutte, S.K., Suzuki, H., Crespo, I., Das, S., Radoeva, T., Fontana, M.,  
883 Yoshitake, Y., Hainiwa, E., van den Berg, W., et al. (2020). Design principles of a  
884 minimal auxin response system. *Nat Plants* **6**, 473–482. 10.1038/s41477-020-0662-y.

885 42. Abel, S., and Theologis, A. (1996). Early Genes and Auxin Action. *Plant Physiol* **111**, 9–  
886 17. 10.1104/pp.111.1.9.

887 43. McClure, B.A., Hagen, G., Brown, C.S., Gee, M.A., and Guilfoyle, T.J. (1989).  
888 Transcription, organization, and sequence of an auxin-regulated gene cluster in  
889 soybean. *Plant Cell* **1**, 229–239. 10.1105/tpc.1.2.229.

890 44. Fendrych, M., Akhmanova, M., Merrin, J., Glanc, M., Hagiwara, S., Takahashi, K.,  
891 Uchida, N., Torii, K.U., and Friml, J. (2018). Rapid and reversible root growth inhibition  
892 by TIR1 auxin signalling. *Nat Plants* **4**, 453–459. 10.1038/s41477-018-0190-1.

893 45. Dindas, J., Scherzer, S., Roelfsema, M.R.G., von Meyer, K., Müller, H.M., Al-Rasheid,  
894 K.A.S., Palme, K., Dietrich, P., Becker, D., Bennett, M.J., et al. (2018). AUX1-mediated  
895 root hair auxin influx governs SCFTIR1/AFB-type Ca<sup>2+</sup> signaling. *Nat Commun* **9**, 1174.  
896 10.1038/s41467-018-03582-5.

897 46. Yoon, H.S., Hackett, J.D., Ciniglia, C., Pinto, G., and Bhattacharya, D. (2004). A  
898 Molecular Timeline for the Origin of Photosynthetic Eukaryotes. *Mol Biol Evol* **21**,  
899 809–818. 10.1093/molbev/msh075.

900 47. Leebens-Mack, J.H., Barker, M.S., Carpenter, E.J., Deyholos, M.K., Gitzendanner, M.A.,  
901 Graham, S.W., Grosse, I., Li, Z., Melkonian, M., Mirarab, S., et al. (2019). One thousand  
902 plant transcriptomes and the phylogenomics of green plants. *Nature* **574**, 679–685.  
903 10.1038/s41586-019-1693-2.

904 48. Jiao, C., Sørensen, I., Sun, X., Sun, H., Behar, H., Alseekh, S., Philippe, G., Palacio Lopez,  
905 K., Sun, L., Reed, R., et al. (2020). The *Penium margaritaceum* Genome: Hallmarks of  
906 the Origins of Land Plants. *Cell* **181**, 1097-1111.e12. 10.1016/j.cell.2020.04.019.

907 49. Ren, H., Park, M.Y., Spartz, A.K., Wong, J.H., and Gray, W.M. (2018). A subset of  
908 plasma membrane-localized PP2C.D phosphatases negatively regulate SAUR-mediated  
909 cell expansion in *Arabidopsis*. *PLoS Genet* **14**, e1007455.  
910 10.1371/journal.pgen.1007455.

911 50. Takahashi, K., Hayashi, K., and Kinoshita, T. (2012). Auxin Activates the Plasma  
912 Membrane H<sup>+</sup>-ATPase by Phosphorylation during Hypocotyl Elongation in  
913 *Arabidopsis*. *Plant Physiol* **159**, 632–641. 10.1104/pp.112.196428.

914 51. Renier, M., Tamanini, A., Nicolis, E., Rolfini, R., Imler, J.-L., Pavirani, A., and Cabrini, G.  
915 (1995). Use of a Membrane Potential-Sensitive Probe to Assess Biological Expression  
916 of the Cystic Fibrosis Transmembrane Conductance Regulator. *Hum Gene Ther* **6**,  
917 1275–1283. 10.1089/hum.1995.6.10-1275.

918 52. Tominaga, M., and Ito, K. (2015). The molecular mechanism and physiological role of  
919 cytoplasmic streaming. *Curr Opin Plant Biol* **27**, 104–110. 10.1016/j.pbi.2015.06.017.

920 53. Huibin Han, Inge Verstraeten, Mark Roosjen, Ewa Mazur, Nikola Rýdza, Jakub Hajný,  
921 Krisztina Ötvös, Dolf Weijers, and Jiří Friml (2021). Rapid auxin-mediated  
922 phosphorylation of Myosin regulates trafficking and polarity in *Arabidopsis*. *bioRxiv*.

923 54. Songyang, Z., Lu, K.P., Kwon, Y.T., Tsai, L.H., Filhol, O., Cochet, C., Brickey, D.A.,  
924 Soderling, T.R., Bartleson, C., Graves, D.J., et al. (1996). A structural basis for substrate  
925 specificities of protein Ser/Thr kinases: primary sequence preference of casein kinases  
926 I and II, NIMA, phosphorylase kinase, calmodulin-dependent kinase II, CDK5, and Erk1.  
927 *Mol Cell Biol* **16**, 6486–6493. 10.1128/MCB.16.11.6486.

928 55. Lewis, T.S., Shapiro, P.S., and Ahn, N.G. (1998). Signal Transduction through MAP  
929 Kinase Cascades. In, pp. 49–139. 10.1016/S0065-230X(08)60765-4.

930 56. (Kazuya Ichimura et al.), M.G., Ichimura, K., Shinozaki, K., Tena, G., Sheen, J., Henry, Y.,  
931 Champion, A., Kreis, M., Zhang, S., Hirt, H., et al. (2002). Mitogen-activated protein  
932 kinase cascades in plants: a new nomenclature. *Trends Plant Sci* **7**, 301–308.  
933 10.1016/S1360-1385(02)02302-6.

934 57. Shahzad, Z., Canut, M., Tournaire-Roux, C., Martinière, A., Boursiac, Y., Loudet, O., and  
935 Maurel, C. (2016). A Potassium-Dependent Oxygen Sensing Pathway Regulates Plant  
936 Root Hydraulics. *Cell* **167**, 87-98.e14. 10.1016/j.cell.2016.08.068.

937 58. Lin, Z., Li, Y., Zhang, Z., Liu, X., Hsu, C.-C., Du, Y., Sang, T., Zhu, C., Wang, Y., Satheesh,  
938 V., et al. (2020). A RAF-SnRK2 kinase cascade mediates early osmotic stress signaling  
939 in higher plants. *Nat Commun* **11**, 613. 10.1038/s41467-020-14477-9.

940 59. Koide, E., Suetsugu, N., Iwano, M., Gotoh, E., Nomura, Y., Stolze, S.C., Nakagami, H.,  
941 Kohchi, T., and Nishihama, R. (2020). Regulation of Photosynthetic Carbohydrate  
942 Metabolism by a Raf-Like Kinase in the Liverwort *Marchantia polymorpha*. *Plant Cell*  
943 *Physiol* **61**, 631–643. 10.1093/pcp/pcz232.

944 60. Bowman, J.L., Kohchi, T., Yamato, K.T., Jenkins, J., Shu, S., Ishizaki, K., Yamaoka, S.,  
945 Nishihama, R., Nakamura, Y., Berger, F., et al. (2017). Insights into Land Plant

946 Evolution Garnered from the *Marchantia polymorpha* Genome. *Cell* 171, 287-304.e15.  
947 <https://doi.org/10.1016/j.cell.2017.09.030>.

948 61. Benková, E., Michniewicz, M., Sauer, M., Teichmann, T., Seifertová, D., Jürgens, G.,  
949 and Friml, J. (2003). Local, Efflux-Dependent Auxin Gradients as a Common Module  
950 for Plant Organ Formation. *Cell* 115, 591–602. 10.1016/S0092-8674(03)00924-3.

951 62. Flores-Sandoval, E., Eklund, D.M., and Bowman, J.L. (2015). A Simple Auxin  
952 Transcriptional Response System Regulates Multiple Morphogenetic Processes in the  
953 Liverwort *Marchantia polymorpha*. *PLoS Genet* 11, e1005207.  
954 10.1371/journal.pgen.1005207.

955 63. Mutte, S.K., and Weijers, D. (2020). Deep Evolutionary History of the Phox and Bem1  
956 (PB1) Domain Across Eukaryotes. *Sci Rep* 10, 3797. 10.1038/s41598-020-60733-9.

957 64. Bienz, M. (2014). Signalosome assembly by domains undergoing dynamic head-to-tail  
958 polymerization. *Trends Biochem Sci* 39, 487–495. 10.1016/j.tibs.2014.08.006.

959 65. Moscat, J., Diaz-Meco, M.T., Albert, A., and Campuzano, S. (2006). Cell Signaling and  
960 Function Organized by PB1 Domain Interactions. *Mol Cell* 23, 631–640.  
961 10.1016/j.molcel.2006.08.002.

962 66. Jakobi, A.J., Huber, S.T., Mortensen, S.A., Schultz, S.W., Palara, A., Kuhm, T., Shrestha,  
963 B.K., Lamark, T., Hagen, W.J.H., Wilmanns, M., et al. (2020). Structural basis of  
964 p62/SQSTM1 helical filaments and their role in cellular cargo uptake. *Nat Commun* 11,  
965 440. 10.1038/s41467-020-14343-8.

966 67. Lamark, T., Perander, M., Outzen, H., Kristiansen, K., Øvervatn, A., Michaelsen, E.,  
967 Bjørkøy, G., and Johansen, T. (2003). Interaction Codes within the Family of  
968 Mammalian Phox and Bem1p Domain-containing Proteins. *Journal of Biological  
969 Chemistry* 278, 34568–34581. 10.1074/jbc.M303221200.

970 68. Nakamura, K., Uhlik, M.T., Johnson, N.L., Hahn, K.M., and Johnson, G.L. (2006). PB1  
971 Domain-Dependent Signaling Complex Is Required for Extracellular Signal-Regulated  
972 Kinase 5 Activation. *Mol Cell Biol* 26, 2065–2079. 10.1128/MCB.26.6.2065-2079.2006.

973 69. Blagoev, B., Ong, S.-E., Kratchmarova, I., and Mann, M. (2004). Temporal analysis of  
974 phosphotyrosine-dependent signaling networks by quantitative proteomics. *Nat  
975 Biotechnol* 22, 1139–1145. 10.1038/nbt1005.

976 70. Winston, B.W., Lange-Carter, C.A., Gardner, A.M., Johnson, G.L., and Riches, D.W.  
977 (1995). Tumor necrosis factor alpha rapidly activates the mitogen-activated protein  
978 kinase (MAPK) cascade in a MAPK kinase kinase-dependent, c-Raf-1-independent  
979 fashion in mouse macrophages. *Proceedings of the National Academy of Sciences* 92,  
980 1614–1618. 10.1073/pnas.92.5.1614.

981 71. Tominaga, M., Kimura, A., Yokota, E., Haraguchi, T., Shimmen, T., Yamamoto, K.,  
982 Nakano, A., and Ito, K. (2013). Cytoplasmic Streaming Velocity as a Plant Size  
983 Determinant. *Dev Cell* 27, 345–352. 10.1016/j.devcel.2013.10.005.

984 72. Du, M., Spalding, E.P., and Gray, W.M. (2020). Rapid Auxin-Mediated Cell Expansion.  
985 *Annu Rev Plant Biol* 71, 379–402. 10.1146/annurev-arplant-073019-025907.

986 73. Folta, K.M., and Spalding, E.P. (2001). Unexpected roles for cryptochrome 2 and  
987 phototropin revealed by high-resolution analysis of blue light-mediated hypocotyl  
988 growth inhibition. *The Plant Journal* 26, 471–478. 10.1046/j.1365-313x.2001.01038.x.

989 74. Kato, H., Ishizaki, K., Kouno, M., Shirakawa, M., Bowman, J.L., Nishihama, R., and  
990 Kohchi, T. (2015). Auxin-Mediated Transcriptional System with a Minimal Set of  
991 Components Is Critical for Morphogenesis through the Life Cycle in *Marchantia*  
992 *polymorpha*. *PLoS Genet* 11, e1005084. 10.1371/journal.pgen.1005084.

993 75. Yu, Y., Tang, W., Lin, W., Zhou, X., Li, W., Li, Y., Chen, R., Cao, W., Perez-Henriquez, P.,  
994 Huang, R., et al. (2022). ABLs and TMKs are co-receptors for extracellular auxin.

995 76. Khuri, S., Bakker, F.T., and Dunwell, J.M. (2001). Phylogeny, Function, and Evolution of  
996 the Cupins, a Structurally Conserved, Functionally Diverse Superfamily of Proteins.  
997 *Mol Biol Evol* 18, 593–605. 10.1093/oxfordjournals.molbev.a003840.

998 77. Murashige, T., and Skoog, F. (1962). A revised medium for rapid growth and bio assays  
999 with tobacco tissue cultures. *Physiol Plant* 15, 473–497.

1000 78. Dai, N., Wang, W., Patterson, S.E., and Bleecker, A.B. (2013). The TMK Subfamily of  
1001 Receptor-Like Kinases in *Arabidopsis* Display an Essential Role in Growth and a  
1002 Reduced Sensitivity to Auxin. *PLoS One* 8, e60990-.

1003 79. Gao, Y., Zhang, Y., Zhang, D., Dai, X., Estelle, M., and Zhao, Y. (2015). Auxin binding  
1004 protein 1 (ABP1) is not required for either auxin signaling or *Arabidopsis* development.  
1005 *Proceedings of the National Academy of Sciences* 112, 2275–2280.  
1006 10.1073/pnas.1500365112.

1007 80. Savaldi-Goldstein, S., Baiga, T.J., Pojer, F., Dabi, T., Butterfield, C., Parry, G., Santner,  
1008 A., Dharmasiri, N., Tao, Y., Estelle, M., et al. (2008). New auxin analogs with growth-  
1009 promoting effects in intact plants reveal a chemical strategy to improve hormone  
1010 delivery. *Proceedings of the National Academy of Sciences* 105, 15190–15195.  
1011 10.1073/pnas.0806324105.

1012 81. Gamborg, O.L., Miller, R.A., and Ojima, K. (1968). Nutrient requirements of suspension  
1013 cultures of soybean root cells. *Exp Cell Res* 50, 151–158. 10.1016/0014-  
1014 4827(68)90403-5.

1015 82. Cove, D.J., Perroud, P.-F., Charron, A.J., McDaniel, S.F., Khandelwal, A., and Quatrano,  
1016 R.S. (2009). Culturing the Moss *Physcomitrella patens*. *Cold Spring Harb Protoc* 2009,  
1017 pdb.prot5136. 10.1101/pdb.prot5136.

1018 83. Domozych, D.S., Sørensen, I., Popper, Z.A., Ochs, J., Andreas, A., Fangel, J.U., Pielach,  
1019 A., Sacks, C., Brechka, H., Ruisi-Besares, P., et al. (2014). Pectin Metabolism and  
1020 Assembly in the Cell Wall of the Charophyte Green Alga *Penium margaritaceum*. *Plant*  
1021 *Physiol* 165, 105–118. 10.1104/pp.114.236257.

1022 84. Perez-Riverol, Y., Bai, J., Bandla, C., García-Seisdedos, D., Hewapathirana, S.,  
1023 Kamatchinathan, S., Kundu, D.J., Prakash, A., Frericks-Zipper, A., Eisenacher, M., et al.  
1024 (2022). The PRIDE database resources in 2022: a hub for mass spectrometry-based  
1025 proteomics evidences. *Nucleic Acids Res* 50, D543–D552. 10.1093/nar/gkab1038.

1026 85. Emms, D.M., and Kelly, S. (2019). OrthoFinder: phylogenetic orthology inference for  
1027 comparative genomics. *Genome Biol* 20, 238. 10.1186/s13059-019-1832-y.

1028 86. Gao, Y., and Kilfoil, M.L. (2009). Accurate detection and complete tracking of large  
1029 populations of features in three dimensions. *Opt Express* 17, 4685.  
1030 10.1364/OE.17.004685.

1031 87. Metzler, R., Jeon, J.-H., Cherstvy, A.G., and Barkai, E. (2014). Anomalous diffusion  
1032 models and their properties: non-stationarity, non-ergodicity, and ageing at the  
1033 centenary of single particle tracking. *Phys. Chem. Chem. Phys.* 16, 24128–24164.  
1034 10.1039/C4CP03465A.

1035 88. Regner, B.M., Vučinić, D., Domnisoru, C., Bartol, T.M., Hetzer, M.W., Tartakovsky,  
1036 D.M., and Sejnowski, T.J. (2013). Anomalous Diffusion of Single Particles in Cytoplasm.  
1037 *Biophys J* 104, 1652–1660. 10.1016/j.bpj.2013.01.049.

1038 89. Serre, N.B., Wernerova, D., Vittal, P., Dubey, S.M., Medvecka, E., Jelinkova, A.,  
1039 Petrasek, J., Grossmann, G., and Fendrych, M. (2022). The AUX1-afb1-CNGC14  
1040 module establishes longitudinal root surface pH profile. *bioRxiv*.

1041 90. Cheng, C., Krishnakumar, V., Chan, A.P., Thibaud-Nissen, F., Schobel, S., and Town,  
1042 C.D. (2017). Araport11: a complete reannotation of the *Arabidopsis thaliana* reference  
1043 genome. *The Plant Journal* **89**, 789–804. 10.1111/tpj.13415.

1044 91. Montgomery, S.A., Tanizawa, Y., Galik, B., Wang, N., Ito, T., Mochizuki, T., Akimcheva,  
1045 S., Bowman, J.L., Cognat, V., Maréchal-Drouard, L., et al. (2020). Chromatin  
1046 Organization in Early Land Plants Reveals an Ancestral Association between  
1047 H3K27me3, Transposons, and Constitutive Heterochromatin. *Current Biology* **30**, 573–  
1048 588.e7. 10.1016/j.cub.2019.12.015.

1049 92. Kim, D., Langmead, B., and Salzberg, S.L. (2015). HISAT: a fast spliced aligner with low  
1050 memory requirements. *Nat Methods* **12**, 357–360. 10.1038/nmeth.3317.

1051 93. Li, H., Handsaker, B., Wysoker, A., Fennell, T., Ruan, J., Homer, N., Marth, G., Abecasis,  
1052 G., and Durbin, R. (2009). The Sequence Alignment/Map format and SAMtools.  
1053 *Bioinformatics* **25**, 2078–2079. 10.1093/bioinformatics/btp352.

1054 94. Liao, Y., Smyth, G.K., and Shi, W. (2014). featureCounts: an efficient general purpose  
1055 program for assigning sequence reads to genomic features. *Bioinformatics* **30**, 923–  
1056 930. 10.1093/bioinformatics/btt656.

1057 95. Love, M.I., Huber, W., and Anders, S. (2014). Moderated estimation of fold change  
1058 and dispersion for RNA-seq data with DESeq2. *Genome Biol* **15**, 550. 10.1186/s13059-  
1059 014-0550-8.

1060 96. de Rybel, B., van den Berg, W., Lokerse, A.S., Liao, C.-Y., van Mourik, H., Möller, B.,  
1061 Llavata-Peris, C.I., and Weijers, D. (2011). A Versatile Set of Ligation-Independent  
1062 Cloning Vectors for Functional Studies in Plants . *Plant Physiol* **156**, 1292–1299.  
1063 10.1104/pp.111.177337.

1064 97. Ishizaki, K., Nishihama, R., Ueda, M., Inoue, K., Ishida, S., Nishimura, Y., Shikanai, T.,  
1065 and Kohchi, T. (2015). Development of Gateway Binary Vector Series with Four  
1066 Different Selection Markers for the Liverwort *Marchantia polymorpha*. *PLoS One* **10**,  
1067 e0138876. 10.1371/journal.pone.0138876.

1068 98. KUBOTA, A., ISHIZAKI, K., HOSAKA, M., and KOHCHI, T. (2013). Efficient *Agrobacterium*  
1069 -Mediated Transformation of the Liverwort *Marchantia polymorpha* Using  
1070 Regenerating Thalli. *Biosci Biotechnol Biochem* **77**, 167–172. 10.1271/bbb.120700.

1071 99. Woo, E.-J. (2002). Crystal structure of auxin-binding protein 1 in complex with auxin.  
1072 *EMBO J* **21**, 2877–2885. 10.1093/emboj/cdf291.

1073

1074

1075

1076

1077 **FIGURE LEGENDS**

1078

1079 **Figure 1 Comparative phosphoproteomics identifies a rapid and conserved auxin**  
1080 **response.** (A) Distribution histograms of significant differential phosphosites (FDR $\leq$ 0.05)  
1081 comparing 2 minutes of 100 nM IAA (Auxin) treatment with mock treatment across 5 species.  
1082 Numbers of hyper- or hypo-phosphorylated sites are indicated. (B) Strategy for orthogroup  
1083 based on protein sequence across the 5 species used here (top). The lower panel shows the  
1084 number proteins residing in shared (black) and unique (grey) orthogroups in each species. (C)  
1085 Venn diagram depicting the orthogroups found as differentially phosphorylated upon auxin  
1086 treatment in all 5 species. (D) Reduced GO analysis (Revigo) of the 29 shared orthogroups  
1087 (marked green in panel C). Circle sizes correspond to gene count within orthogroups. (E)  
1088 Heatmap depicting measured significantly differential phosphosites (FDR $\leq$ 0.05) of two  
1089 kinase families, PHOT and RAF-like kinases. (F) Venn diagram depicting the number of  
1090 shared GO terms across all species tested, based on closest *Arabidopsis* homolog of each  
1091 differential protein (FDR $\leq$ 0.05). (G) Reduced GO analysis (Revigo) of the 7 shared  
1092 orthogroups (marked green in panel F). (H) Differential phosphorylation of plasma membrane  
1093 H<sup>+</sup>-ATPases across all species tested.

1094

1095 **Figure 2 Auxin triggers fast cellular and physiological responses across the plant**  
1096 **kingdom**

1097 (A) Scheme depicting membrane polarity and depolarization measured using DISBAC2(3)  
1098 fluorescence (left) and normalized fluorescence in control (mock) and IAA-treated  
1099 *Arabidopsis* root cells, *Marchantia* thallus cells and *Klebsormidium* cells. (B) Scheme  
1100 depicting cytoplasmic streaming (left) and diffusion rate K ( $\mu\text{m}^2/\text{s}$ ) in control (mock) and  
1101 IAA-treated *Arabidopsis* root cells and *Marchantia* thallus. Boxplots are shown along  
1102 individual measurements, number of observations (n) is indicated, and significance (Student's  
1103 t-test) is shown.

1104

1105 **Figure 3. Identification of MARK/RAF-like kinases.**

1106 (A) Clustering of phosphomotif enrichment scores (using motifR) of significantly  
1107 differential (FDR $\leq$ 0.05) phosphosites in all tested species. (B) Raw MS1 intensities of RAF-  
1108 like kinase orthologues in mock- and IAA-treated samples. Phosphorylated residues are

1109 indicated. Lower: domain topology of B4 RAF-like kinases indicating positions of PB1 and  
1110 kinase domains (residue numbers) in *Arabidopsis* MARK5/Raf24 (At), *Marchantia*  
1111 MARK/PRAF (Mp), *Physcomitrium* MARK (Pp) and *Klebsormidium* MARK (Kn). **(C)**  
1112 Inferred phylogeny of the B4 RAF-like kinase. *Arabidopsis* numbering is indicated on the top.  
1113 Every node represents an inferred ancestral gene copy at each divergence event. The complete  
1114 tree can be found at interactive Tree of Life (iTOL): <https://itol.embl.de/shared/dolfweijers>.  
1115 **(D)** Phenotype of *Arabidopsis* (left) Col-0 wild-type and *mark/raf* null mutant rosettes and  
1116 *Marchantia* (right) Tak-1 wild-type and *mark/praf* mutants thallus **(E,F)** Length of Col-0  
1117 wild-type and *mark/raf* mutant *Arabidopsis* roots **(E)** and area of Tak-1 wild-type and  
1118 *mark/praf* mutant *Marchantia* thallus **(F)** on increasing concentrations of IAA. Distributions at  
1119 each concentration were tested for significant differences using ANOVA.  
1120

1121 **Figure 4. MARK mediates auxin phosphoresponse across land plant species.**

1122 **(A,B)** PCA plots (left) and expression analysis of individual, auxin-regulated genes (right)  
1123 from RNA-seq analysis on (Col-0; Tak-1) wildtype and *mark* mutants in *Arabidopsis* roots  
1124 and *Marchantia* gemmae treated with 1 $\mu$ M IAA for 1 hour. **(C)** Distribution histograms of  
1125 significant differential phosphosites (FDR $\leq$ 0.05) comparing 2 minutes of 100 nM IAA  
1126 (Auxin) treatment with mock treatment in wild-type (dashed lines) and *mark* mutant (solid  
1127 area) *Arabidopsis* roots (top) and *Marchantia* gemmae (bottom). Number of phosphosites is  
1128 indicated. **(D)** Venn diagrams indicating orthogroup overlap of significantly differential  
1129 phosphosites (FDR $\leq$ 0.05) in *mark* mutants in *Arabidopsis* and *Marchantia* compared to  
1130 respective wild-types under mock condition. **(E)** Venn diagrams indicating orthogroup  
1131 overlap of significantly differential phosphosites (FDR $\leq$ 0.05) in *mark* mutants and wild-types  
1132 in *Arabidopsis* and *Marchantia* under IAA-treated condition. **(F)**. Gene ontology analysis on  
1133 the overlapping and conserved auxin- and MARK-dependent proteins. **(G,H)** Heatmap  
1134 showing differential phosphorylation in *Arabidopsis* **(G)** and *Marchantia* **(H)** *mark* mutants of  
1135 all kinases that are auxin-regulated in wild-type.  
1136

1137 **Figure 5. Requirements of MARK activation and activity**

1138 **(A)** Heatmap showing phosphorylation profiles, normalized to the t=0 timepoint, of  
1139 *Arabidopsis* MARK/RAF kinases (data from Roosjen-Kuhn et.al., accompanying  
1140 manuscript). Profiles marked with asterisk and red name are phosphosites located in the  
1141 activation loop. **(B)** Chord plot depicting overlap between significant (FDR $\leq$ 0.05)

1142 phosphosites in *Arabidopsis* mutants challenged with auxin (red) or without (blue). Overlap  
1143 shows that the *mark/raf* mutant shares more commonly regulated phosphosites with *tmk1-1*  
1144 and *abp1-TD1* mutants than with the *afb1-3* mutant. **(C)** Z-scored MS1 intensities off all  
1145 measured phosphosites of *Arabidopsis* MARK/RAF kinases in wild-type, *afb1-3*, *tmk1-1* and  
1146 *abp1-TD1* mutants with or without IAA. **(D)** Principal component analysis of Z-scored MS1  
1147 intensities of all 1048 phosphosites that are auxin-regulated in wild-type in control- and  
1148 auxin-treated wildtype, *tmk1-1*, *abp1-TD1* and *afb1-3* mutants.

1149

1150 **Figure 6 MARK links rapid phospho-response to fast auxin responses**

1151 **(A)** Fluorescence of *Arabidopsis* MARK5/RAF20-TurboID-sYFP, driven from its  
1152 endogenous promoter, in primary root tips. Right panel shows close-up of epidermal cells. **(B)**  
1153 Fluorescence of *Marchantia* MARK/PRAF-Citrine driven from its endogenous promoter in  
1154 gemma. Right panel shows close-up of rhizoid initial cells. **(C)** Analysis of membrane  
1155 depolarization on *Arabidopsis* and *Marchantia* *mark* mutants in mock and IAA-treated root  
1156 (Arabidopsis) and thallus (*Marchantia*) cells (compare to Figure 2 A for wild types).  
1157 Displayed is the normalized DISBAC2(3) fluorescence (IAA/mock). **(D)** Cytoplasmic  
1158 streaming in *Arabidopsis* and *Marchantia* *mark* mutants in mock and IAA-treated root  
1159 (Arabidopsis) and thallus (*Marchantia*) cells (compare to Figure 2B for wild types). Displayed  
1160 is the Diffusion rate K ( $\mu\text{m}^2/\text{s}$ ). Boxplots are shown along individual measurements, number  
1161 of observations (n) is indicated, and significance (Student's t-test) is shown.

1162

1163 **Supplementary figure 1. Cytoplasmic streaming relies on the actin cytoskeleton (A,B)**  
1164 Quantification of the diffusive component ( $\alpha$ ) of cytoplasmic streaming in wild-type and  
1165 *mark/raf* mutant *Arabidopsis* roots **(A)** and wild-type and Atmark/praf mutant *Marchantia*  
1166 thallus **(B)** with and without auxin treatment. **(C,D)** Diffusive Exponent ( $\alpha$ ; C) and Diffusion  
1167 Rate (K; D) of cytoplasmic streaming in wild-type *Arabidopsis* roots treated with mock  
1168 medium or Lantrunculin B. Boxplots are shown along individual measurements, number of  
1169 observations (n) is indicated, and significance (Student's t-test) is shown.

1170

1171

1172 **Supplementary figure 2 Phenotypic analysis of *mark* mutants in *Marchantia* and**  
1173 ***Arabidopsis***

1174 (A) Projected thallus area in wild-type and *Mpmark/praf*<sup>ko</sup> mutant *Marchantia* thallus,  
1175 followed over 29 days. (B) Number of gemma cup on wild-type and *Mpmark/praf*<sup>ko</sup> mutant  
1176 *Marchantia* thallus. (C). Root length in wild-type and *mark/raf*<sup>null</sup> mutant *Arabidopsis*  
1177 seedlings, followed over 9 days. (D,E) Rosette area (D) and height (E) in wild-type and  
1178 *mark/raf*<sup>null</sup> mutant *Arabidopsis* plants. (F) Germination rate of wild-type and *mark/raf*<sup>null</sup>  
1179 mutant *Arabidopsis* seeds, followed over 9 days. (G,H) Examples of images used for  
1180 quantification in panel A and C, respectively.

1181

1182 **Supplementary figure 3: Analysis of *mark* mutant phosphoproteomes.**

1183 (A) Overlap of MARK targets in *Arabidopsis* and *Marchantia*, based on differential  
1184 phosphorylation in *Atmark/raf* and *Mpmark/praf* phosphoproteomes under mock conditions,  
1185 compared to wild-types. (B) Venn diagram showing overlap between phosphosites  
1186 differentially regulated ( $\leq 0.05$ ) in mannitol-treated *Arabidopsis* plants (Lin et.al. 2020),  
1187 100nM IAA treated Col-0 and 100nM treated *mark* null mutant. (C) Gene identifiers of  
1188 *Arabidopsis* MARK/Raf kinases.

1189

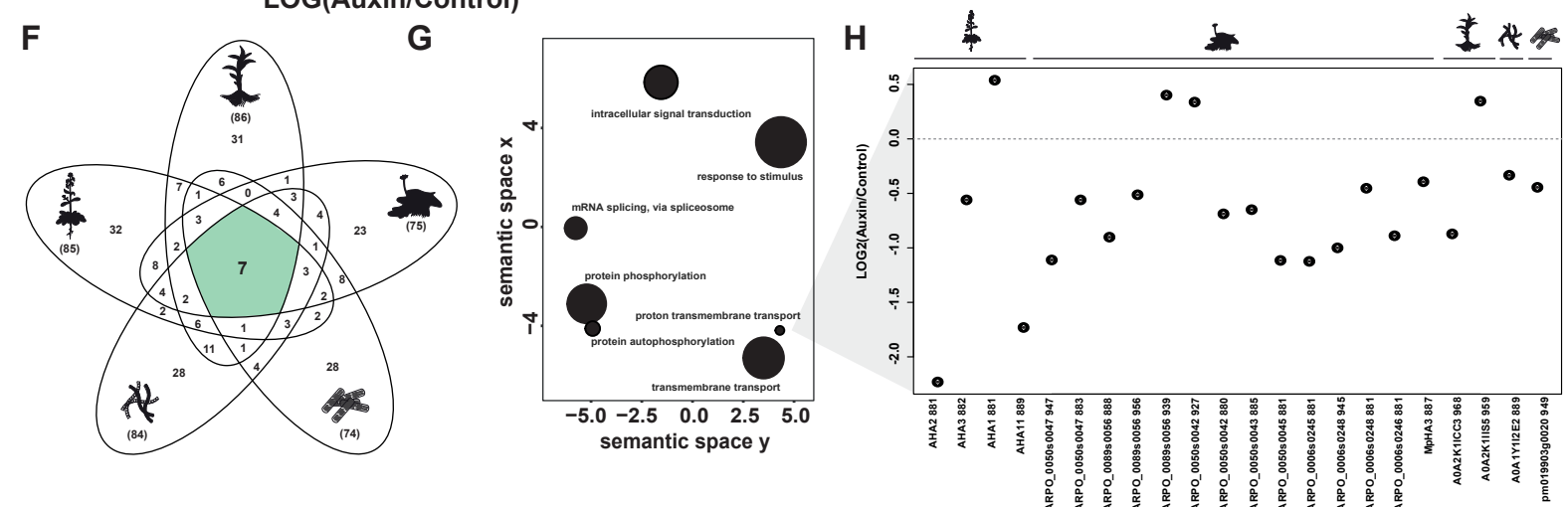
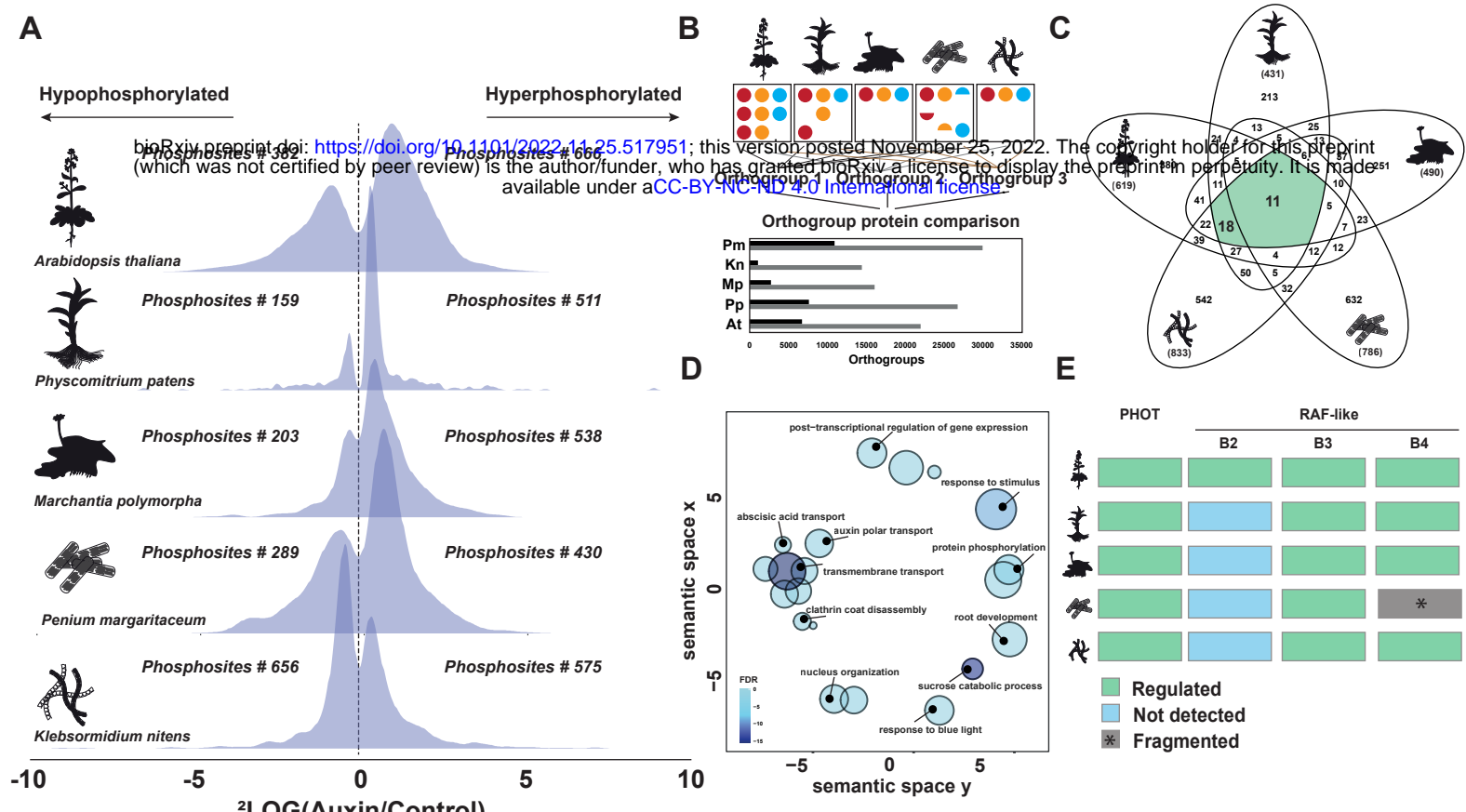
1190 **Supplementary Figure 4: Dynamics of membrane potential in wild-type and *mark/raf***  
1191 ***mutant Arabidopsis* roots**

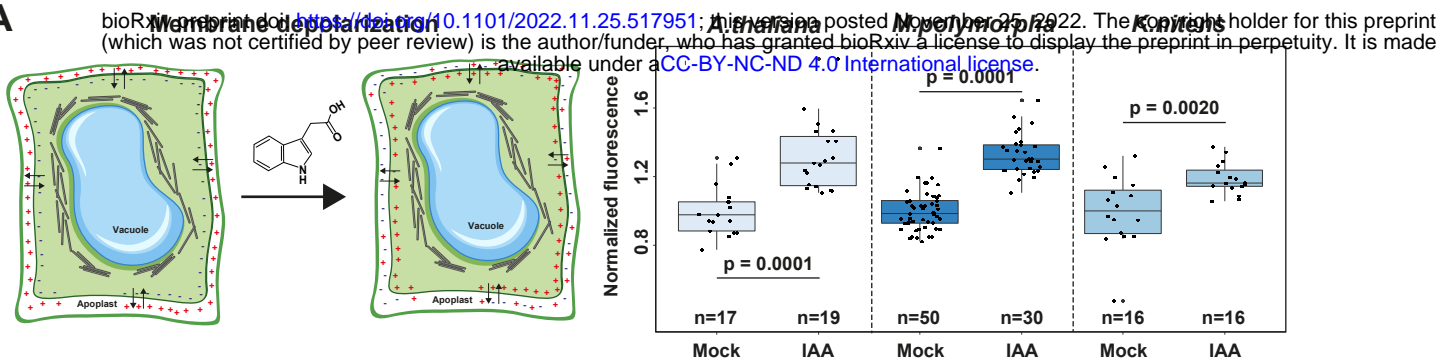
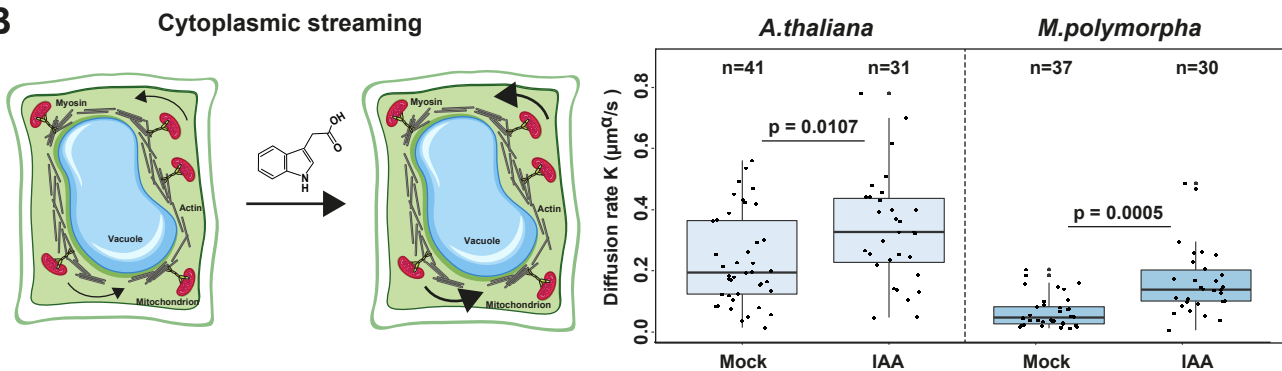
1192 (A) *Arabidopsis* wildtype (Col-0) and *mark/raf*<sup>null</sup> mutant root surface pH visualized using the  
1193 ratiometric pH-sensitive FS dye treated with mock or 100 nM IAA; scale bar = 50  $\mu$ m. (B)  
1194 Quantification of the F488/405 nm fluorescence emission ratio along the root surface of  
1195 wildtype (Col-0) and *mark/raf*<sup>null</sup>. Higher ratio corresponds to alkaline pH. Control and 100  
1196 nM IAA-treated roots are shown. The graphs show the averages 12 and 11 roots for wildtype  
1197 (Col-0) and *mark/raf*<sup>null</sup>, respectively for both mock and IAA conditions. Shaded areas  
1198 represent standard deviations. (C) Dynamics of membrane potential after treatment with 100  
1199 nM IAA (arrow) in *Atmark/raf*<sup>null</sup> (n=10), Col-0 (n=6) and *afb1-3* (n=6) roots. Membrane  
1200 potential was visualized by the relative change of the DISBAC2(3) fluorescence over time in  
1201 a microfluidic chip. Average values are shown, shaded areas represent standard deviations.

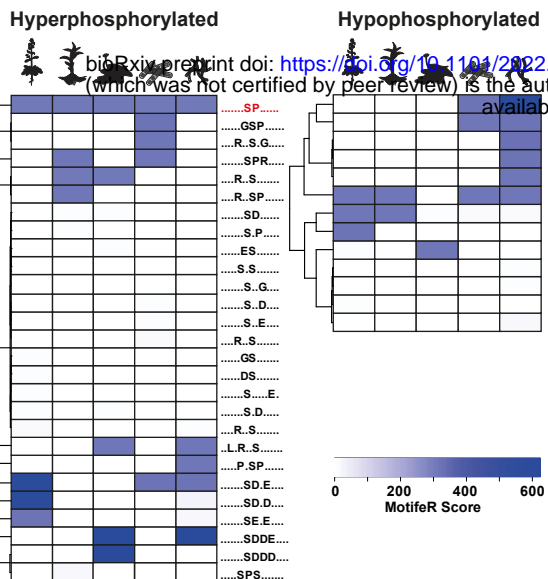
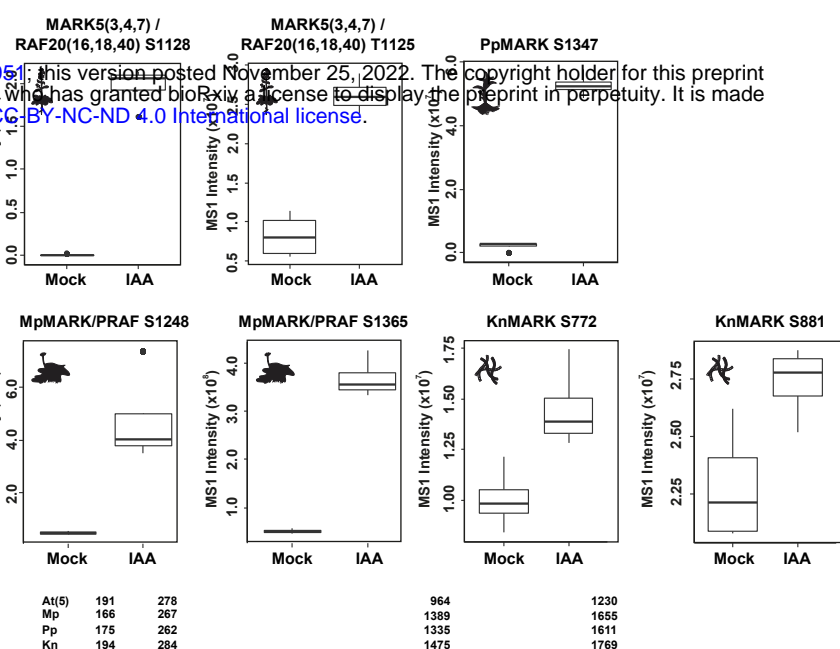
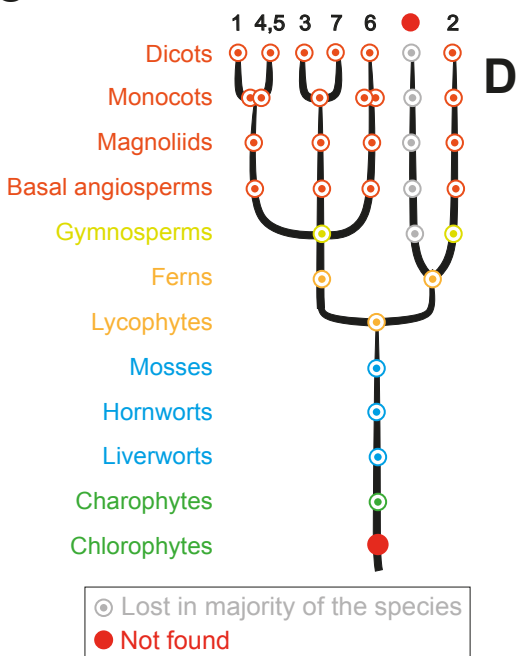
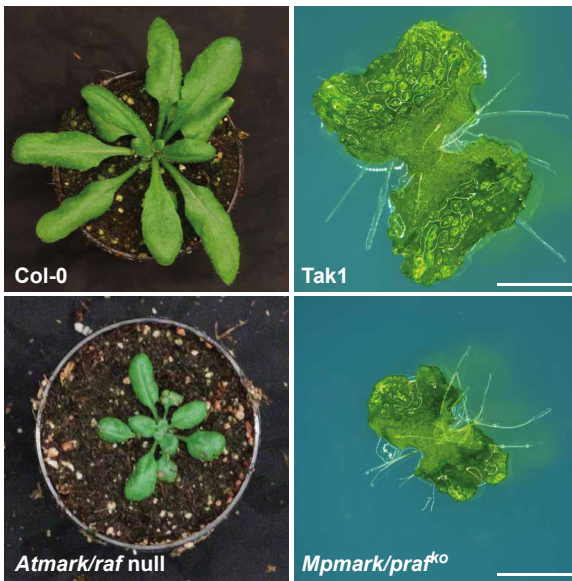
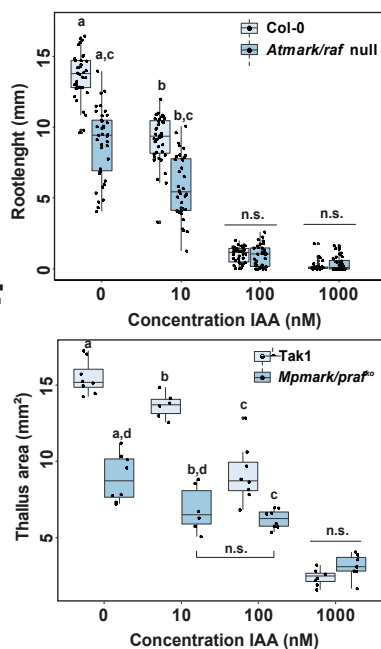
1202

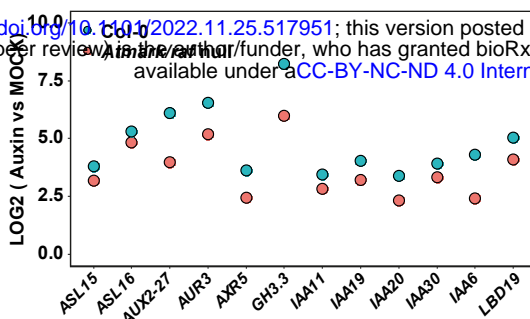
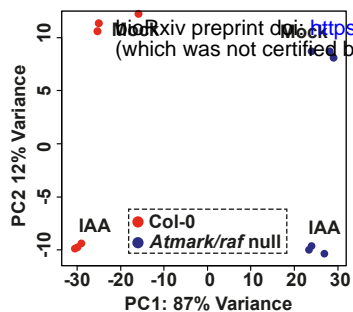
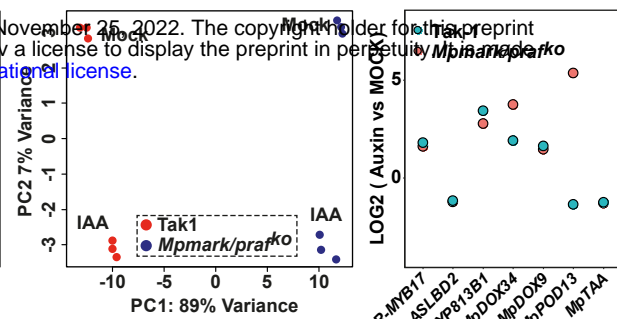
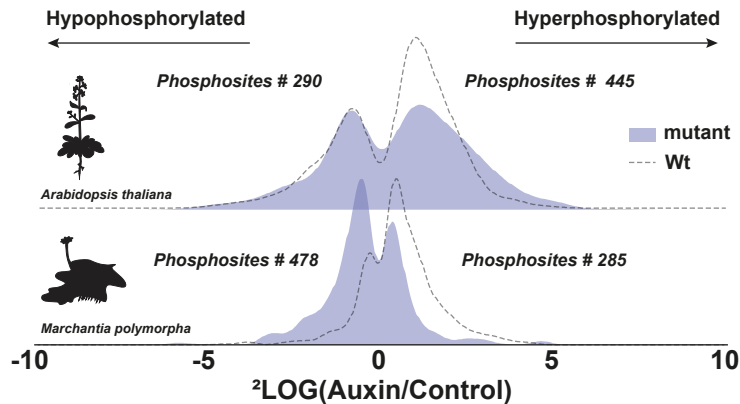
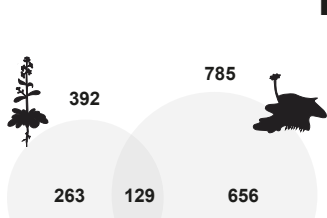
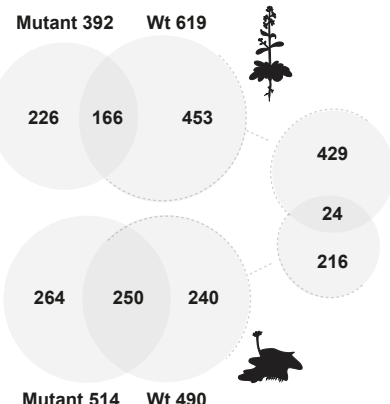
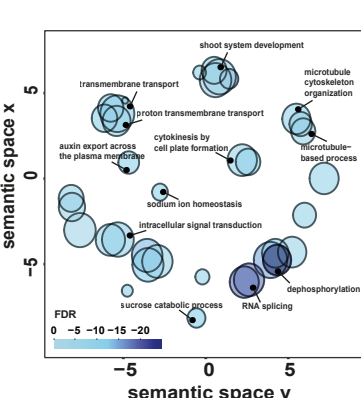
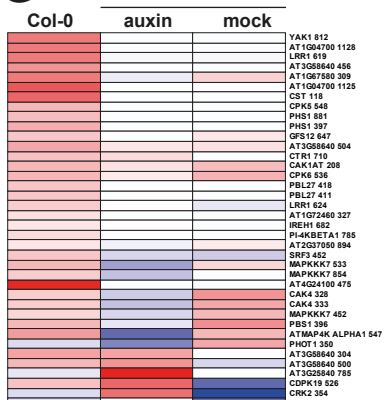
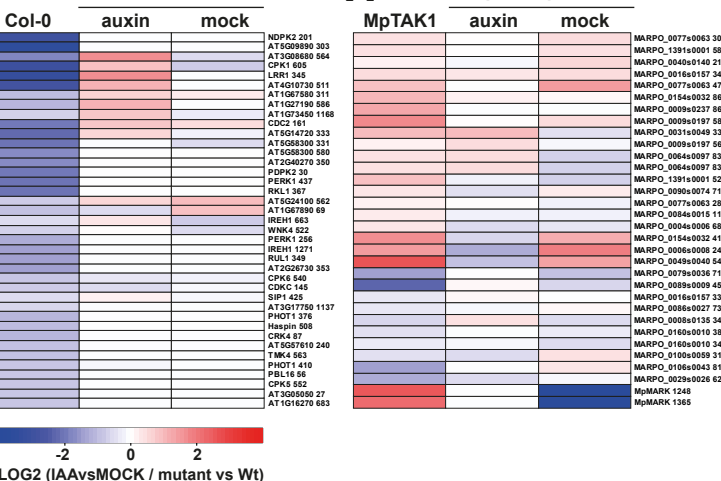
1203 **Supplementary figure 6 Phylogenetic analysis of ABP1.**

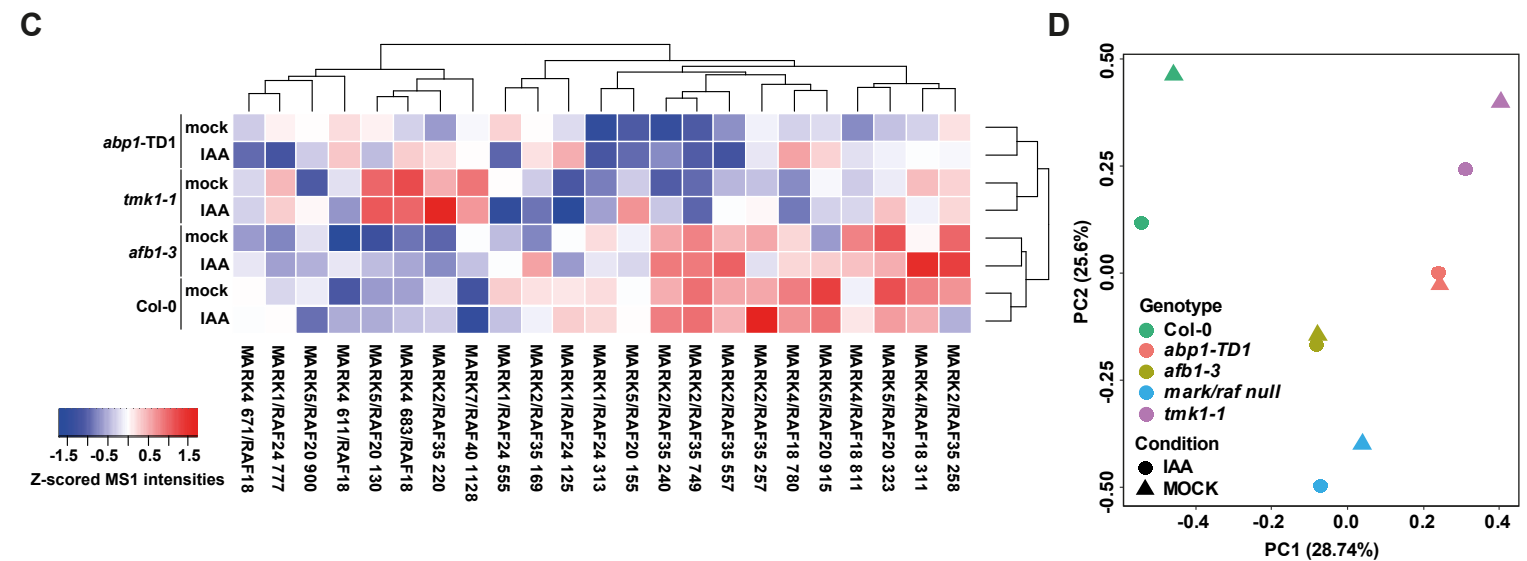
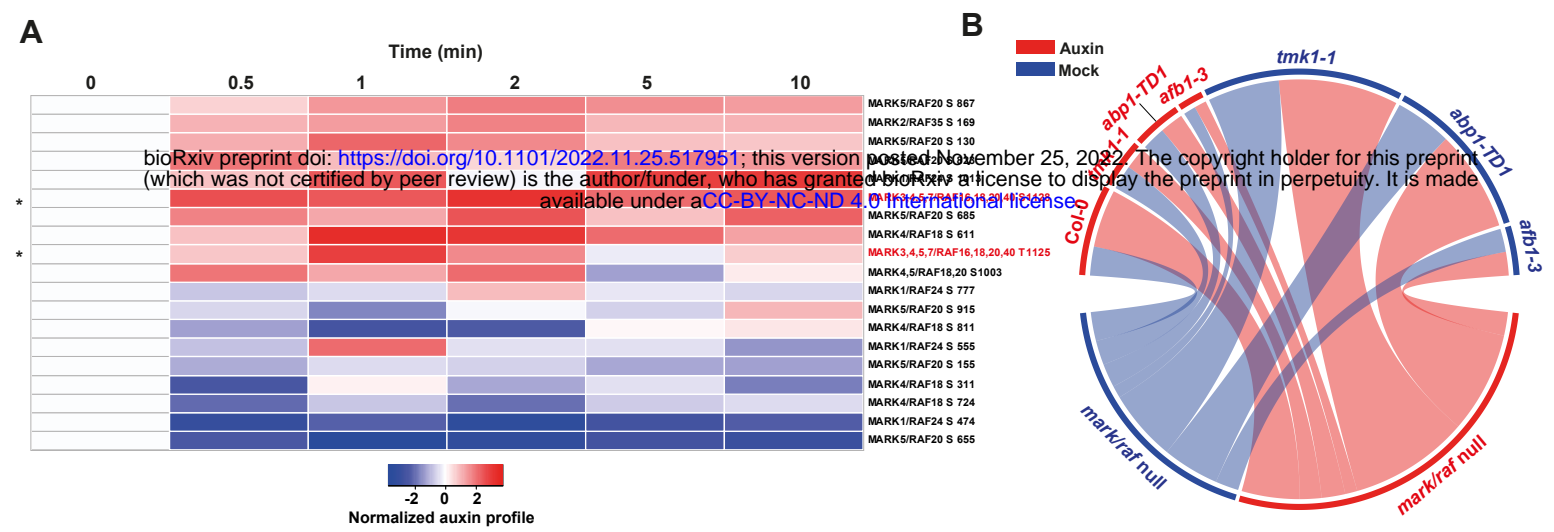
1204 (A) Phylogenetic tree of the ABP1 gene family with green algae and land plant homologs.  
1205 Branches that are well-supported (bootstrap >75) are marked with dots. Orthologs from each  
1206 phylum are represented with a different color. (B) Deep conservation of key amino acids in  
1207 the ABP1 auxin binding pocket, as well as the Zinc binding site. Light blue to dark blue color  
1208 gradient represents low to high conservation, respectively. Numbering on the top is based on  
1209 maize ABP1 protein <sup>99</sup>. The complete tree can be found at interactive Tree of Life (iTOL):  
1210 <https://itol.embl.de/shared/dolfweijers>.



**A****B**

**A****B****C****D****E****F**

**A****B****C****D****E****F****G****H**

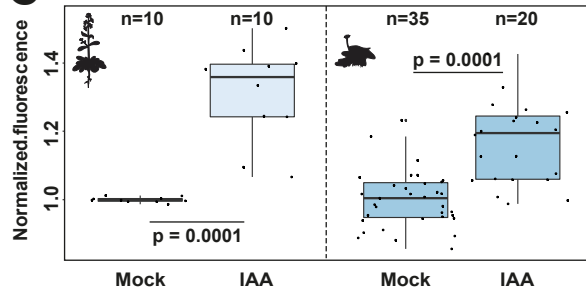


**A**

bioRxiv preprint doi: <https://doi.org/10.1101/2022.11.25.517951>; this version posted November 25, 2022. The copyright holder for this preprint (which was not certified by peer review) is the author/funder, who has granted bioRxiv a license to display the preprint in perpetuity. It is made available under a [aCC-BY-NC-ND 4.0 International license](https://creativecommons.org/licenses/by-nd/4.0/).

**B**

bioRxiv preprint doi: <https://doi.org/10.1101/2022.11.25.517951>; this version posted November 25, 2022. The copyright holder for this preprint (which was not certified by peer review) is the author/funder, who has granted bioRxiv a license to display the preprint in perpetuity. It is made available under a [aCC-BY-NC-ND 4.0 International license](https://creativecommons.org/licenses/by-nd/4.0/).

**C****D**